First-time comparison between NO_2 vertical columns from GEMS and Pandora measurements

Serin Kim[1], Daewon Kim[1], Hyunkee Hong[2], Lim-Seok Chang[2], Hanlim Lee[1], Deok-Rae Kim[2], Donghee Kim[2], Jeong-Ah Yu[2], Dongwon Lee[2], Ukkyo Jeong[1], Chang-Kuen Song[3], Sang-Woo Kim[4], Sang Seo Park[3], Jhoon Kim[5], Thomas F. Hanisco[6], Junsung Park[1], Wonei Choi[1], Kwangyul Lee[7]

[1]Division of Earth Environmental System Science, Major of Spatial Information Engineering, Pukyong National University, Busan, Republic of Korea
[2]Environmental Satellite Center, National Institute of Environmental Research, Incheon, Republic of Korea
[3]Department of Urban & Environmental Engineering, Ulsan National Institute of Science and Technology, Ulsan, Republic of Korea
[4]School of Earth and Environmental Sciences, Seoul National University, Seoul, Republic of Korea
[5]Department of Atmospheric Sciences, Yonsei University, Seoul, Republic of Korea
[6]Atmospheric Chemistry and Dynamics Lab, NASA Goddard Space Flight Center, Greenbelt, MD, USA
[7]Air Quality Research Division, Climate and Air Quality Research Department, National Institute of Environmental Research, Incheon, Republic of Korea

Correspondence to: Daewon Kim (k.daewon91@gmail.com)

Abstract. The Geostationary Environmental Monitoring Spectrometer (GEMS) is a UV–visible spectrometer onboard the GEO-KOMPSAT-2B satellite launched into a geostationary orbit in February 2020. To evaluate the GEMS NO_2 total column data, a comparison was carried out using the NO_2 vertical column density (VCD) measured using direct- sunlight using observations by the Pandora spectrometer system at four sites in Seosan, South Korea, fromduring November 2020 to January 2021. Correlation coefficients between GEMS and Pandora NO_2 data at four sites ranged from 0.35 to 0.48, with root mean square errors (RMSEs) from 4.7×10^{15} molec. cm^{-2} to 5.5×10^{15} molec. cm^{-2} for cloud fraction (CF) < 0.7. Higher correlation coefficients of 0.62–0.78 with lower RMSEs from 3.3×10^{15} molec. cm^{-2} to 4.3×10^{15} molec. cm^{-2} were found with CF < 0.3, indicating the higher sensitivity of GEMS to atmospheric NO_2 in less-cloudy conditions. Overall, the GEMS NO_2 total column data tended to be lower than those of Pandora owingdue to differences in representative spatial coverage, with a large negative bias under high-CF conditions. With a correction for horizontal representativeness in Pandora measurement coverage, the correlation coefficients ranginge from 0.69 to 0.81 with RMSEs from 3.2×10^{15} molec. cm^{-2} to 4.9×10^{15} molec. cm^{-2} were achieved for CF < 0.3, showing the better correlation with the correction than that without the correction.

1 Introduction

Nitrogen dioxide (NO_2) is a key species in the troposphere and stratosphere for atmospheric chemistry and air quality (Crutzen, 1979; Seinfeld and Pandis, 1998), andwhich is mainly emitted by anthropogenic sources, such as fossil fuel combustion in vehicles and power plants. Natural sources, such as lightning, biomass burning, and soil microbial action are also major contributors to atmospheric NO_2 (Crutzen, 1979). NO_2 is a precursor of tropospheric ozone, aerosols, and ~~the~~ hydroxyl radical (OH) (Boersma et al., 2009), and high concentrations affect the lifetime of atmospheric CH_4 and direct radiative forcing of the atmosphere (Pinardi et al., 2020). In addition, the NO_2 diurnal cycles are important factors for understanding temporal patterns such as NOx emissions, chemistry, deposition, advection, diffusion, and convection (Li et al., 2021).

Therefore, it is important to monitor NO_2, and representative methods for this are as follows. Chemiluminescence-based in-situ instruments have provided a highly accurate NO_2 mixing ratio at a measurement location, but with limited spatial coverage (e.g., Bechle et al., 2013; Jeong and Hong, 2021). Satellite-based remote sensing instruments on polar orbits, such as the GOME-1/2 (Global Ozone Monitoring Experiment; Burrows et al., 1999; Munro et al., 2016), SCIAMACHY (Scanning Imaging Spectrometer for Atmospheric Cartography; Bovensmann et al., 1999), OMI (Ozone Monitoring Experiment; Levelt et al., 2006), and TROPOMI (TROPOspheric Monitoring Instrument; Veefkind et al. 2012), have effectively complemented the ground-based observations by providing global distribution of NO_2 total column density (Lamsal et al., 2014). The recently ~~launched~~ GEMS (Geostationary Environment Monitoring Spectrometer; Kim et al., 2020) onboard the GEO-KOMPSAT-2B (Geostationary Korea Multi-Purpose Satellite 2B) was launched in February 2020.~~provides diurnal variations of the NO_2 VCD during daytime over Asia since February 2020.~~ The NIER (National Institute of Environment Research), where the GEMS ground station is operated, has been transmitting the GEMS products including NO_2 Vertical column density (~~column~~ VCD) in real time from December 2022. GEMS Map of the Air Pollution (GMAP) campaigns have taken place from 2020 and are also scheduled to be held annually to evaluate the quality of the GEMS ~~by the~~ measurements of trace gas and aerosol products based on trace gases, aerosol composition and optical property measurements at various platforms. This study conducted the first quick evaluation via comparison between the GEMS NO_2 ~~column data~~VCDs and those of Pandora measurements at several sites in a suburban area in Korea during the first GMAP campaign in 2020 winter. We evaluate the differences between NO_2 VCD obtained from Pandora and GEMS especially depending on cloudy and clear sky conditions.

The c~~C~~omparison and validation of ~~the~~ satellite-based NO_2 VCD retrievals are essential ~~due to~~ because of their non-negligible error sources such as assumed atmospheric profiles, surface reflectance, and measurement uncertainties (Hong et al., 2017). In addition, ~~the diurnal~~ NO_2 VCD retrievals from ~~the~~ GEMS require precise assessments because~~as~~ the observation geometries of the geostationary Earth orbit (GEO) are different from those of the low earth orbits (LEO) and other systematic uncertainties may affect the retrievals (e.g., diurnal variations of the atmospheric profiles, which are used for ~~the~~ air mass factor (AMF) calculations). Ground-based remote sensing instruments such as the MAX-DOAS (multi-axis differential optical absorption spectroscopy; Honninger et al., 2004) measure~~s~~ scattered sunlight at various elevation angles to derive tropospheric column amounts of NO_2 as well as ~~the~~ profile estimates (e.g., Irie et al., 2008; Wagner et al., 2011; Wang et al., 2017). Direct-Sun instruments such as the Pandora (Herman et al., 2009) measure direct sunlight to retriev~~eal~~e the NO_2 VCD, of which the absorption light path of the photons reaching to their detector may be shorter than those of the MAX-DOAS instruments;~~,~~ thus, they are less sensitive to the surface mixing ratio of ~~the~~ NO_2. However, uncertainties in NO_2 VCD retrievals by AMF calculation are low as they use simple geometric AMF~~from the Pandora and direct-sun DOAS have lower uncertainty of the AMF calculations as they utilize simple geometric AMF, whereas that for the MAX-DOAS algorithms take into account the~~

atmospheric profiles as well as the Raman scattering (Herman et al., 2009). Numerous studies have utilized the recently expanding Pandonia Gglobal Nnetwork of Pandora (PGN; https://www.pandonia-global-network.org/) for validation of comparison of the polar-orbiting satellite products (e.g., Herman et al., 2009; Tzortziou et al., 2014, 2015; Herman et al., 2019; Judd et al., 2019, 2020; Pinardi et al., 2020; Verhoelst et al., 2021).

This study represents the first attempt to compare and validate NO_2 VCD retrievals from the GEMS with the Pandora instruments deployed during the GMAP (GEMS Map of the Air Pollution; from November 2020 to January 2021) campaign inaround Seosan, South Korea. Seosan is a sub-urban area, and while the second campaign compared and validated at multiple sites from mega-city to sub-urban characteristics using Pandora and MAX-DOAS after this campaign. The measurement periods and locations of the four Pandora instruments used in this study are summarized in Fig.ure 1 and Table 1. In Section 2, the explanation of campaign and used GEMS data are explaineddescribed, followed by the Pandora instrument and retrieval methodology. Section 3 provides a method of comparison between the instruments and between Pandora and GEMS. The rResults are described in three parts in Section 4: intercomparison between Pandora instruments, the results of comparison with GEMS NO_2, and considerationing of horizontal representativeness. Finally, the conclusions are provided in Section 5.

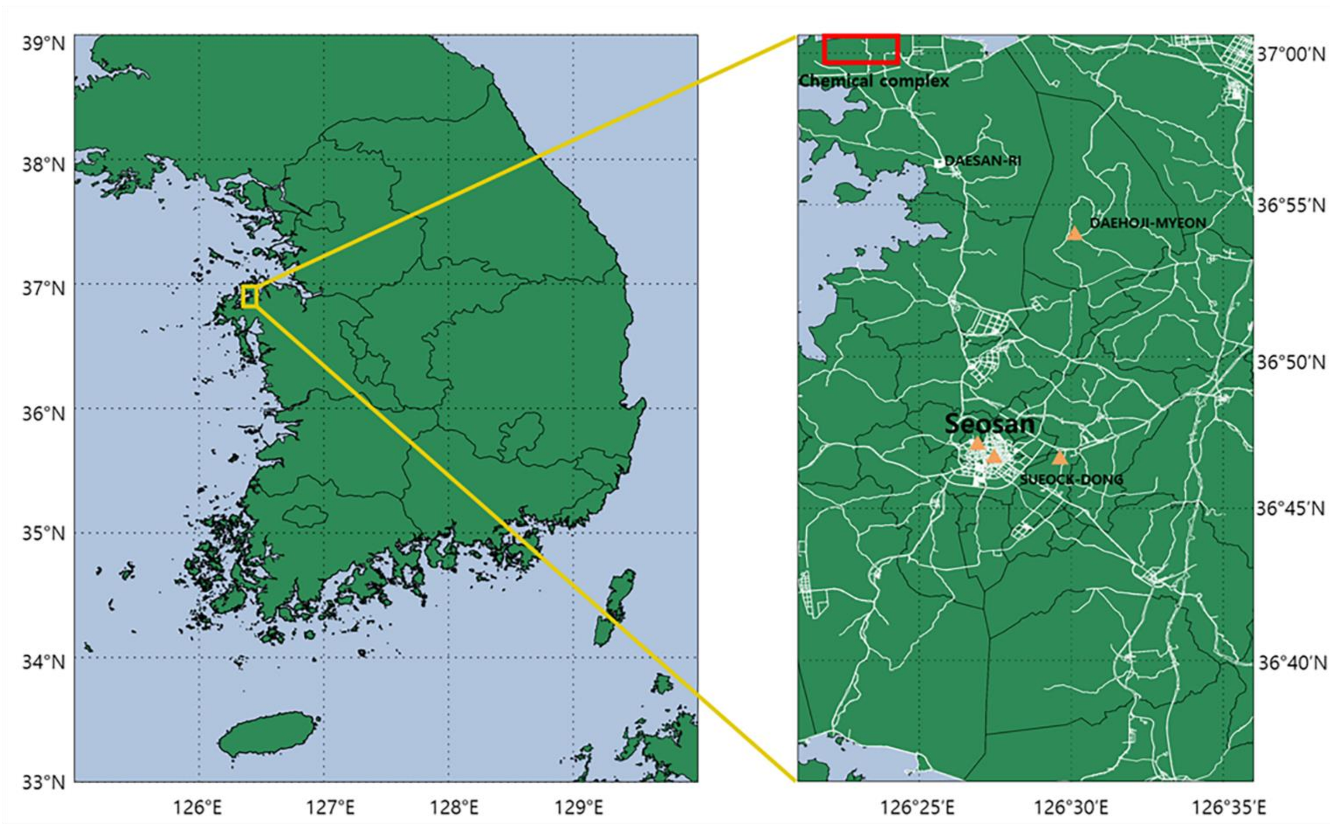

Figure 1. Measurement sites for the GMAP 2020 campaign. Triangles indicate observation sites

Table 1. The ~~information of~~ measurement sites and period.

	Latitude	Longitude	P~~p~~eriod
Seosan (SS)	36.78° N	126.49° E	2020.11.12–2020.12.03 2020.12.03–2021.01.27
Seosan-CC (CC)	36.78° N	126.45° E	2020.12.09–2021.01.31
Daehoji (DHJ)	36.90° N	126.50° E	2020.12.09–2021.01.17
Dongmoon-2dong (DM2)	36.78° N	126.46° E	2020.12.09 – 2021.01.03

2 GMAP campaign

2.1 The first GMAP campaign

~~GMAP 2020,~~ T~~t~~he first GEMS validation campaign, GMAP 2020, was conducted between ~~during~~ November 2020 and~~to~~ January 2021 in Seosan ~~city~~. The Pandora instruments used in the campaign were ~~of~~ the standard versions described in Section. 3.1. The mean NO_2 concentration in~~at~~ Seosan for 2016–2020 was 0.017 ppm, ~0.16 % lower than the Korean national five-year average (https://www.airkorea.or.kr/web, last access: 07 March 2021). ~~Measurements of~~ D~~d~~irect sunlight measurements were conducted~~carried out~~ at four sites, as described in Table 1 and Fig.1: Seosan (SS), Seosan City Council (CC), Dongmun-2dong (DM2), and Daehoji (DHJ). Emissions from vehicular and point sources may have contributed to variations in NO_2 concentrations in the Pandora lines of sight, depending on the wind direction. Major roads and an agricultural complex wer~~ar~~e located within ~0.7 km of the SS site,~~;~~ a road and roundabout we~~a~~re near the CC site~~;~~, a road was~~is~~ near the DM2 site,~~;~~ and a petrochemical complex wa~~i~~s located approximately ~~~~~16 km NW of the DHJ site. To estimate the differences in the NO_2 VCD among the Pandora instruments, an initial intercomparison was conducted for two weeks at the SS site. It should ~~needs to~~ be noted that the Pandora instruments were manufactured with~~by~~ the same optics and spectrograph. However, it is still important to quantify the differences between the NO_2 columns retrieved from the four Pandoras at the~~a~~ same location before ~~we~~ comparing~~e~~ them with the GEMS NO_2. ~~From December 2020 to January 2021, the~~ I~~i~~nstruments were installed at the~~s above~~ four sites to~~for~~ ~~the~~ measure~~ment of~~ direct sunlight from December 2020 to January 2021. The m~~M~~easurement periods varied according~~owing~~ to the instrument conditions (Table 1).

2.2 GEMS NO_2 data

~~The~~ GEMS, a hyperspectral UV-Vis image spectrometer covers a wavelength range of 300–500 nm with a full width at half ~~at~~ maximum (FWHM) of approximately ~~about~~ 0.6 nm. GEMS measures atmospheric concentrations of species that affect air quality, such as NO_2, O_3, SO_2, HCHO, and aerosols on an hourly basis from 00:45 to 05:45 UTC with a spatial resolution of 3.5 × 8 km (Kim et al., 2020). The GEMS NO_2 column retrieval ~~i~~was based on the DOAS algorithm (Platt and Stutz, 2008) at wavelength intervals of 432–450 nm (Park et al., 2020). The GEMS cloud fraction (CF) is retrieved using O_2-O_2 absorption properties and DOAS (Choi et al., 2020). We used CF for the comparison of NO_2 VCDs (more details, see Sect. 3). For ~~the purpose of the~~ data evaluation, we used GEMS L2 NO_2 VCD version 1.0, which ~~were~~ was available immediately after the IOT (in Orbit Test) carried out in July ~~in~~ 2020.

2.3 Pandora Instrument and Spectral Fitting

Pandora is a ground-based spectrometer ~~which~~ that measures direct sunlight over ~~the~~ a wavelength range of 280~~ nm to~~ –525 nm with a FWHM of approximately ~~about~~ 0.6 nm. The c~~C~~harge-coupled device (CCD) detector~~, which is equipped~~ in the Pandora spectrometer ~~consists of~~has 2048×64 pixels. The spectrometer is connected to a telescope ~~so called~~ "head sensor" consisting of a collimator and filters such as UV340 filter, neutral density filters, and opaque filter through an optical fiber with a 400 µm core diameter. A target area can be observed with a field of view (FOV) of up to 1.6° (Herman et al., 2018). The four instruments used here are referred to as P1, P2, P3, and P4. The measured spectra were analyz~~s~~ed to retrieve NO_2 slant column densities (SCD) using QDOAS software (Fayt et al., 2011) based on the DOAS technique~~.~~ which can retrieve trace gas concentrations by separating trace gas absorption cross section into slowly and rapidly varying parts (Honninger et al., 2004). The reference spectrum used for fitting was measured at around noon on a clear day (Herman et al., 2009). This refers to the spectrum with lowest NO_2 concentration used to perform optical density fitting over a period of time. During the intercomparison, the radiance obtained at the noon ~~time~~ on~~f~~ November 28 (a clear day) was used as the reference spectrum for P1, P3, and P4. ~~Here, a reference spectrum denotes a spectrum with least amount of NO_2 presence to carry out optical density fitting during a certain period.~~ November 14 was used as a reference for P2 due to the lack of data on day~~the~~ 28th. As the NO_2 differential VCD (dVCD) from P2 ~~were~~ was retrieved using different reference spectrum, ~~they wer~~it was~~e~~ considered secondary data. The NO_2 differential slant column density (dSCD) was obtained using the absorption cross-sections for NO_2 (254.5K) ~~generated~~ calculated using 220K and 294K (Vandaele et al., 1998) and O_3 (225K) (Serdyuchenko et al., 2014), as a fourth-order polynomial in fitting window of 400–~~-~~440 nm. The wavelength range and absorption cross-section were the same as those used in ~~Pandonia Global Network (~~PGN~~)~~ (https://pandora.gsfc.nasa.gov/, last access: 28 March 2022). ~~We~~ A~~a~~dditionally, we used O_4 at 293K (Thalman and Volkamer, 2013) for the spectral fitting (see Fig. 2). This reduced retrieval error~~s~~ by about 0.2 %. Figure ~~3 presents~~2 shows an example of the P1 spectrum fitting results~~ deconvolution of the P1 spectral fitting~~ at 10:43 Local Time (LT) on November 28, 2020. The NO_2 VCD wa~~i~~s obtained by dividing the NO_2 SCDs by the geometric AMFs. After the initial intercomparison~~ period~~, the reference spectrum was selected when the weather wa~~i~~s clear with no air pollution, because~~as~~ the instrument locations were different. P1 and P4 used noon spectrum on January 14, 2021, as a reference spectrum, whereas P2 and P3 used spectra from December 19, 2020.

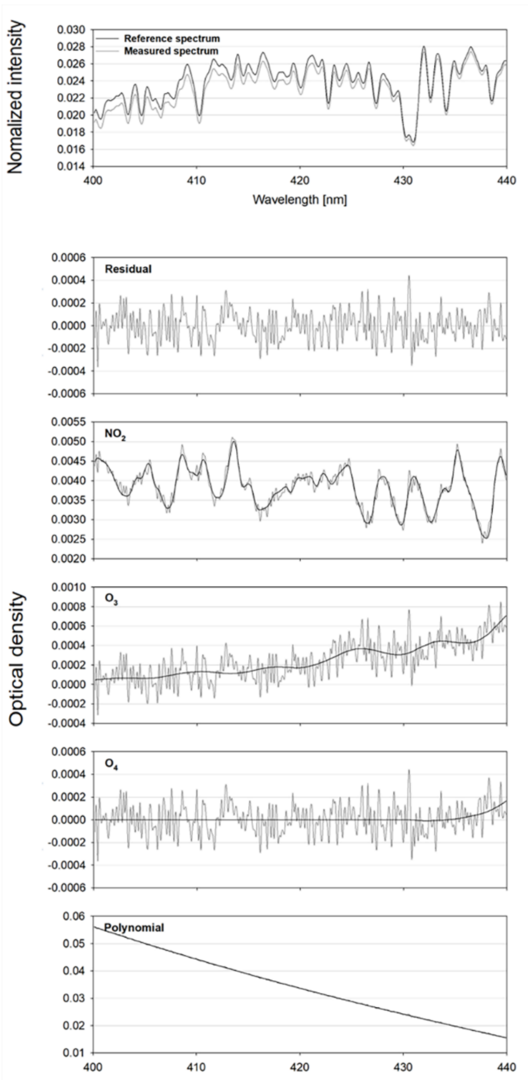

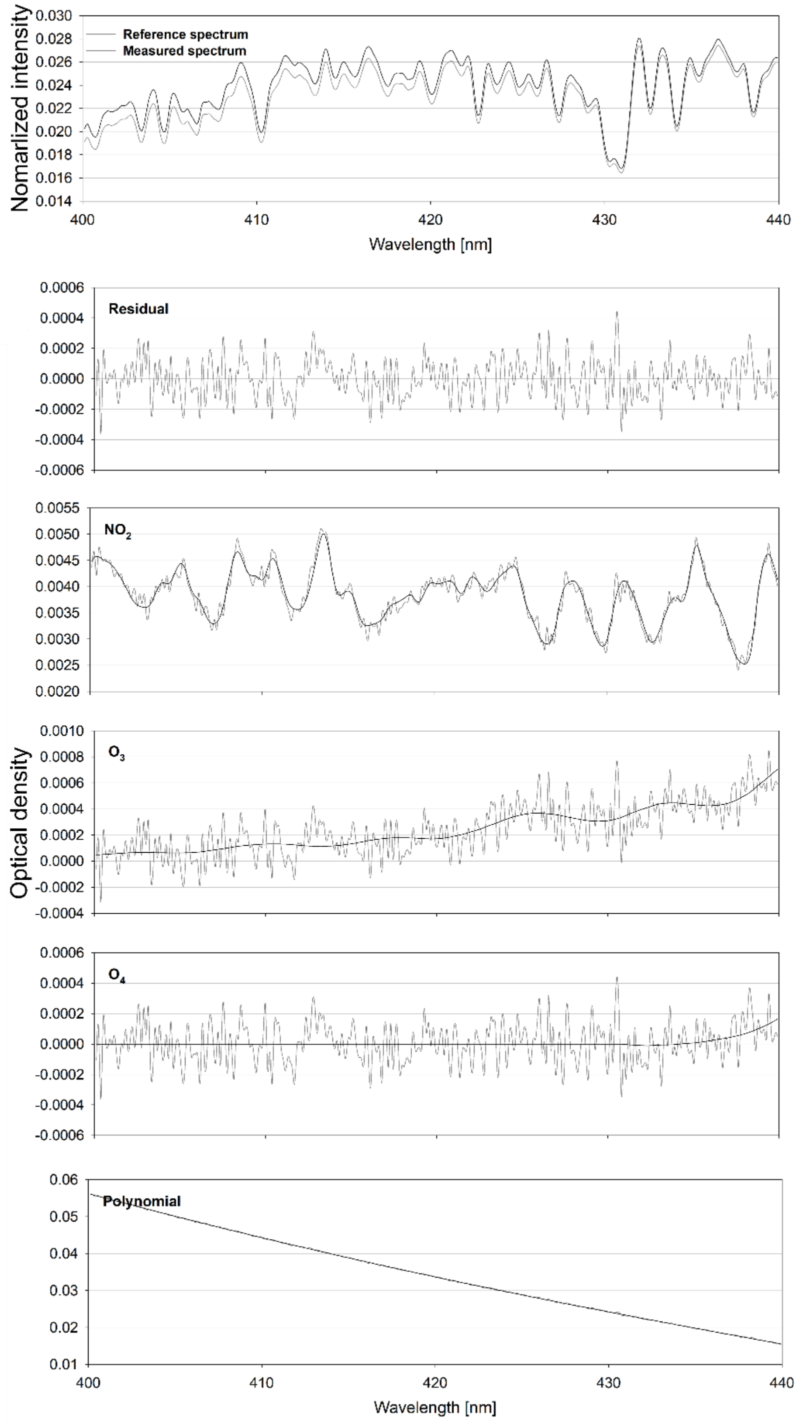

Figure 2. ~~A deconvolution~~Fitted slant column optical depths example for November 28 2020 at 10:43:37 LT for P1. The black line represents the absorption signal, and the grey line represents the absorption signal and fit residual.

3 Method

T~~he purpose of t~~his study aimed~~is~~ to evaluate the GEMS NO_2 ~~column data~~VCD via quick comparisons between the GEMS NO_2 column data and those of Pandora -data~~measurements~~. The differences between the Pandora and GEMS NO_2 data can be attributed to ~~the~~ uncertainties in~~of~~ the Pandora and GEMS NO_2 columns and differences in the measurement geometries. The spatiotemporal differences between the Pandora and GEMS measurements also cause differences between the NO_2 column data obtained from th~~os~~e two ~~different~~ platforms. To quantify the differences in the Pandora NO_2 measurements, all four Pandoras performed identical direct sun measurements at the SS site during the intercomparison period by setting the same observation schedules for all instruments. ~~Differences between the Pandora~~ The NO_2 retrievals from the four collocated Pandora instruments showed consistency of the processed data as shown in Fig. 3 and 4. ~~partially reflects the uncertainties of Pandora NO_2 column data. In order to quantify the differences of the Pandora NO_2 measurements, all four Pandoras performed the identical direct Sun measurements at the SS site during the intercomparison period by setting the same observation schedules for the all instruments.~~ The specifications and retrieval methods ~~of~~ for Pandora are described in Sect. 2.3. During the intercomparison, because clear days were not sufficient to calculate the background concentration, we compared the Pandora instruments using dVCD. On the other hand, in the comparison with GEMS NO_2, NO_2 VCDs from the Pandora were used. As~~Since~~ it measures direct sunlight, it is negligibly affected by ~~the~~ scattered sunlight. However, under~~in~~ cloudy conditions, all Pandora may not see the same location of ~~S~~sun because of~~due to~~ the ~~an~~ inhomogeneity of cloud thinness. In thick cloudy conditions compared with ~~those of~~ clear sky condition, ~~Pandora increases an exposure time to acquire strong enough radiance intensities, which~~ it may lead to the inclusion of unwanted stray light and increase detector noise. T~~In order t~~o understand the influence of ~~the~~ clouds, Pandora was investigated using GEMS cloud fraction (CF) to determine whether the signal was affected by clouds.~~to see whether the signal was affected or not from clouds using GEMS cloud fraction (CF).~~

4 Results

4.1 The intercomparison of NO_2 dVCD from Pandora

~~The~~ Pandora intercomparison was carried out from~~during~~ ~~12~~ November 12 to ~~3~~ December 3, 2020, at the SS site to quantif~~t~~y NO_2 ~~differential VCD (~~dVCD~~)~~ retrievals from the Pandora instruments. We defined dVCD as ~~the~~ differential SCD~~-~~-divided AMF~~g~~ with no background correction.

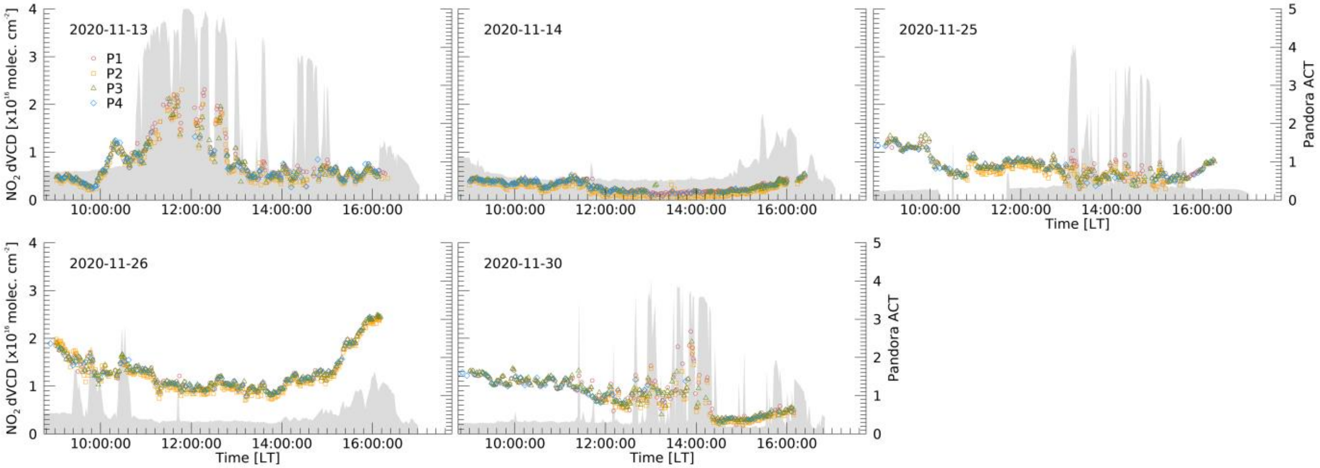

Figure 3. Time series of Pandora retrievals during the intercomparison. Circle (red), square (orange), triangle (green) and diamond (blue) symbols represent total NO_2 dVCD for P1, P2, P3, and P4, respectively. Grey shade represents Pandora aerosol cloud thickness.

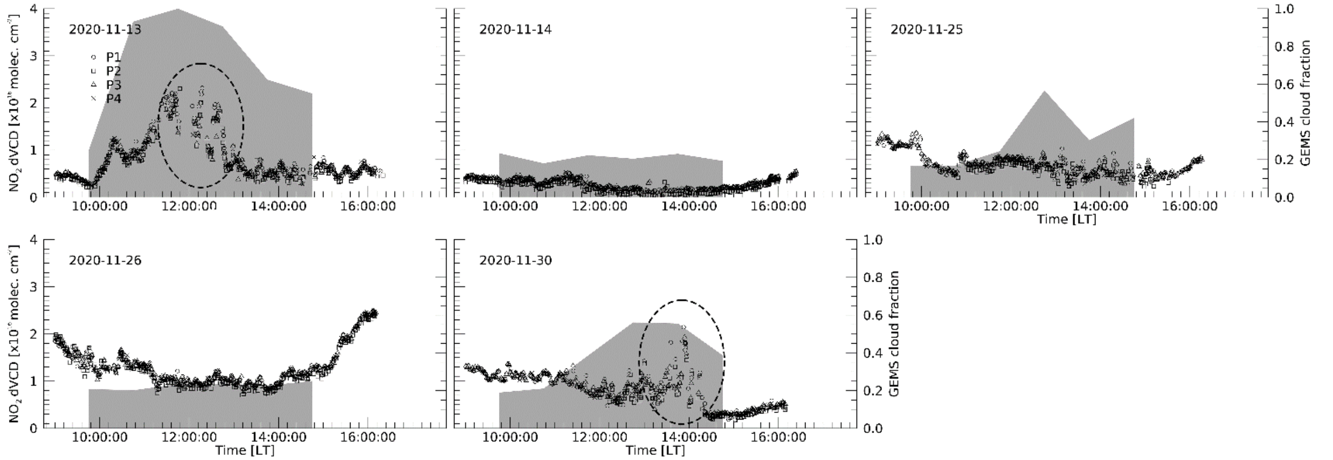

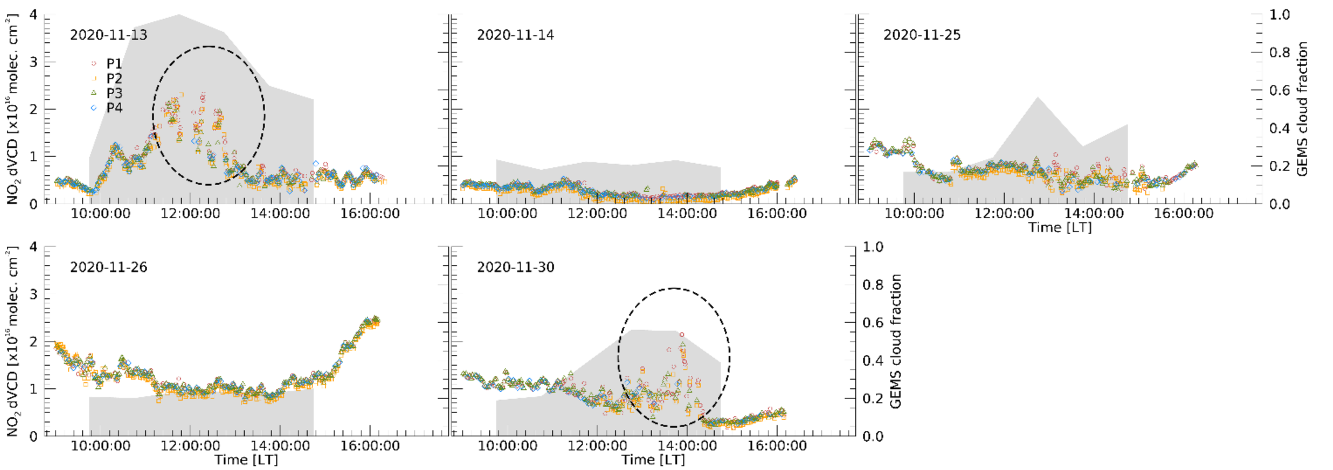

Figure ~~3~~4. Time series of Pandora retrievals during the intercomparison. Circle (red), square (orange), triangle (green) and diamond (blue)~~X~~ symbols represent total NO_2 dVCD for P1, P2, P3, and P4, respectively. Grey shade represents the GEMS cloud fraction.

The time series of data from all instruments for the intercomparison period are shown in Fig. 3 and 4, except for the rainy days. C~~The c~~ircles, squares, triangles, and ~~X~~diamond symbols represent the NO_2 dVCD retrieved by P1, P2, P3, and P4, respectively.~~,~~ ~~and t~~The grey area in Fig. 3 represents the Pandora aerosol cloud thickness (ACT), which indicate the Aerosol Optical depth (AOD) before cloud screening. ACT was retrieved with the Spectral Measurements for Atmospheric Radiative Transfer spectroradiometer (SMART-s) algorithm developed for aerosol retrieval using optimal estimation method (OEM) (Jeong et al., 2020). The diurnal patterns of NO_2 for each Pandora instruments showed good agreement. The NO_2 dVCD during the period ranged from 1.63×10^{14} molec. cm^{-2} to 2.49×10^{16} molec. cm^{-2}, and tend to increase during the morning and late afternoon (after 16:00). At midday, emissions are relatively lower than those during rush hour that have NO_2 emissions from vehicles (Zhao et al., 2020). As Seosan is a sub-urban area, it can be affected by commuting time. As shown in Fig. 3, although there was a good agreement between the instruments, discrepancies occurred in some cases. This occurs when there are many clouds with ACT greater than about 2.5. It is considered that clouds contributed to the discrepancies, which shows certain cloud effects on the NO_2 retrievals from the ground-based direct sun measurements. Thus, aerosols and clouds can affect the retrieval accuracy of trace gases. Therefore, when comparing with GEMS, GEMS CF was used to consider the effects of clouds. Before comparison with GEMS, GEMS CF was also applied during the intercomparison, and can be seen in Fig. 4. The grey area in Fig. 4 represents the GEMS ~~the~~ CF of the GEMS observation time ~~(Fig. 3)~~. ~~The diurnal pattern of NO_2 between each Pandora showed good agreement. The NO_2 VCD during the period ranged from 1.63×10^{14} molec. cm^{-2} to 2.49×10^{16} molec. cm^{-2}, tend to increase during the morning and late afternoon (after 16:00).~~ The dashed-line ovals (Fig. 4~~3~~) indicate periods with discrepancies between the Pandora instruments during the afternoons of~~n~~ November 13 and 30, similar to the case of ~~likely~~ the ACT retrieved from Pandora measurements.~~due to cloud effects, as GEMS CFs were > 0.3 at the time. It is considered that the cloud contributed to the discrepancies since the GEMS CFs were higher than 0.3 on the dates with the discrepancies, which shows certain cloud effects on the NO_2 retrievals from the ground-based direct Sun measurements.~~ Although the temporal trends of ACT and GEMS CF were similar, there is difference in spatiotemporal resolution. The GEMS spatial resolution is 3.5 × 8 km_2, and the measurement area of Pandora could be clear sky even if GEMS retrieved high CF. These differences sometimes result in less spread of Pandora NO_2 for CF > 0.3. Thus, we ~~have carried out the comparisons~~compared ~~between the~~ NO_2 VCDs from Pandora and those from GEMS depending on the CF conditions less than 0.3, 0.5, and 0.7~~, respectively~~. Figure 5 shows the linear regression of the NO_2 dVCDs from P2, P3, and P4 against those from P1, ~~during the intercomparison period,~~ which produced the smalle~~a~~st fitting errors on~~in~~ average during the intercomparison period.

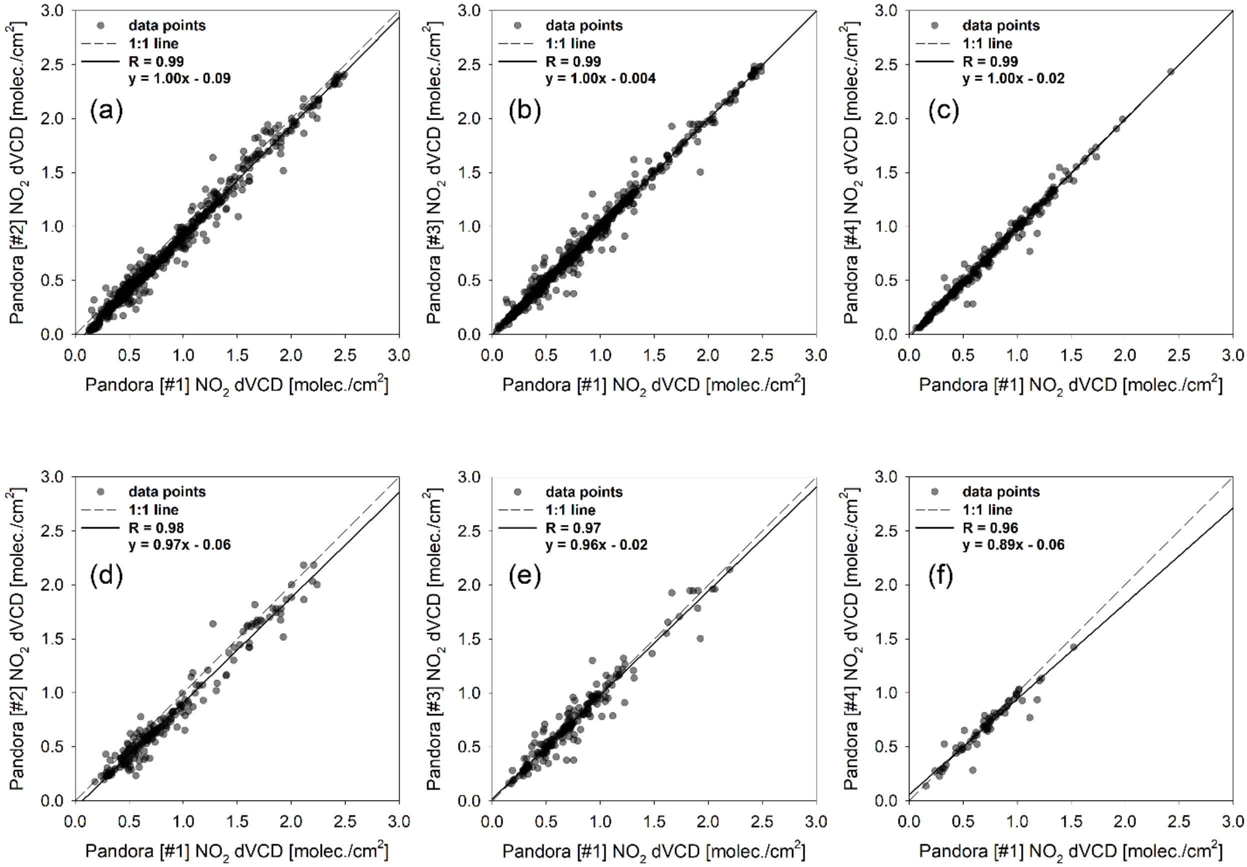
data points
1:1 line
R = 0.99
y = 1.00x - 0.09
(a)
Pandora [#2] NO2 dVCD [molec./cm2]
Pandora [#1] NO2 dVCD [molec./cm2]
data points
1:1 line
R = 0.99
y = 1.00x - 0.004
(b)
Pandora [#3] NO2 dVCD [molec./cm2]
Pandora [#1] NO2 dVCD [molec./cm2]
data points
1:1 line
R = 0.99
y = 1.00x - 0.02
(c)
Pandora [#4] NO2 dVCD [molec./cm2]
Pandora [#1] NO2 dVCD [molec./cm2]
data points
1:1 line
R = 0.98
y = 0.97x - 0.06
(d)
Pandora [#2] NO2 dVCD [molec./cm2]
Pandora [#1] NO2 dVCD [molec./cm2]
data points
1:1 line
R = 0.97
y = 0.96x - 0.02
(e)
Pandora [#3] NO2 dVCD [molec./cm2]
Pandora [#1] NO2 dVCD [molec./cm2]
data points
1:1 line
R = 0.96
y = 0.89x - 0.06
(f)
Pandora [#4] NO2 dVCD [molec./cm2]
Pandora [#1] NO2 dVCD [molec./cm2]

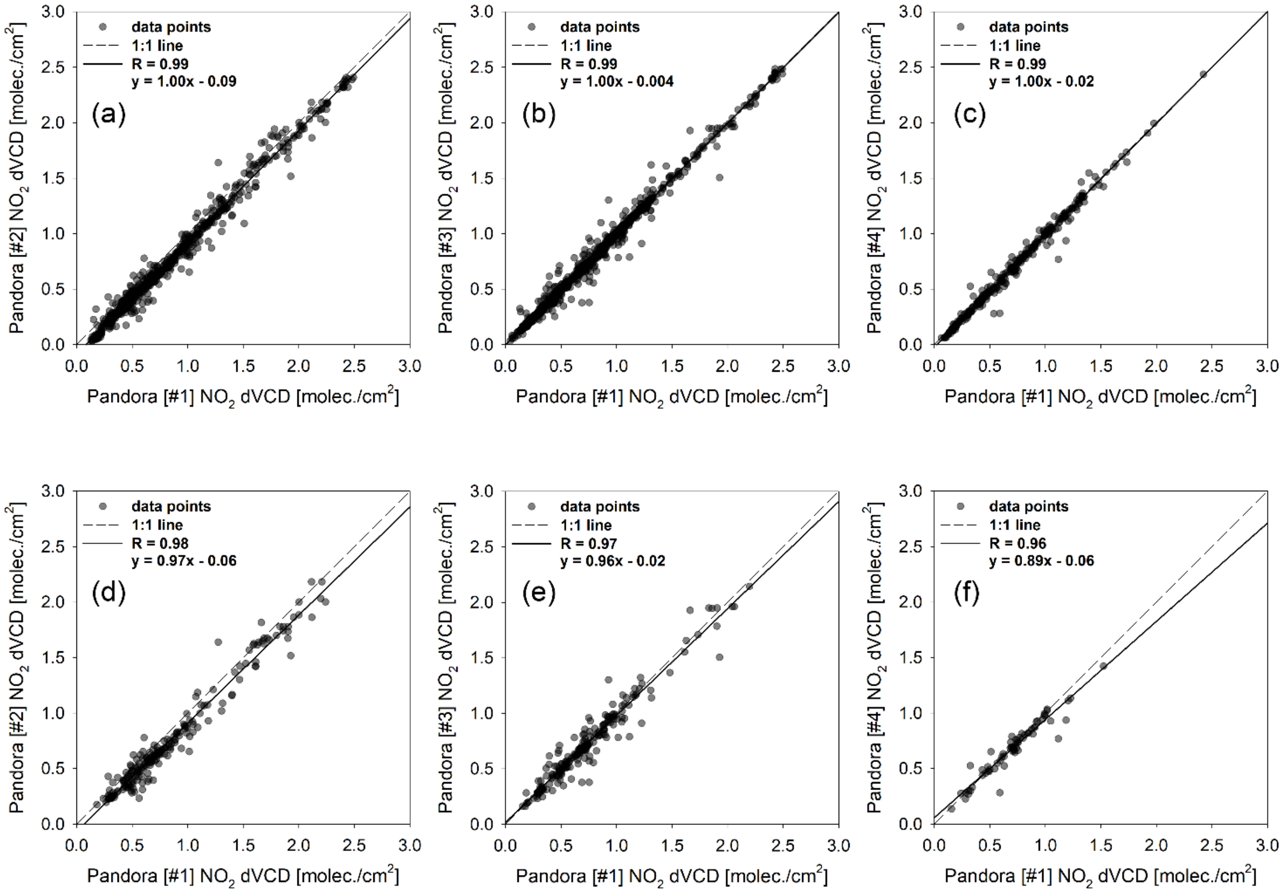

Figure 54. The scatter plots between P1 and others. (a), (b) and (c) shows comparison with all data of P2, P3 and P4. (d), (e) and (f) shows comparison with P2, P3 and P4 when GEMS CF > 0.3.

In Figure 54 a, b, and c, the correlation coefficients were found to be 0.99 with the a slope of 1 and the an interceptor between 0.004– and 0.09, showing the good agreement for all CF conditions. Overall, the NO_2 retrieved by each instrument yielded similar correlations, even with CF > 0.3, although the R values were slightly lower in Fig. 45 d–f, with slopes deviating further from the 1:1 line.

4.2 Comparison of NO_2 VCD between Pandora and GEMS

After the intercomparison period, the Pandora instruments were moved to the four sites for the observation of direct sunlight to evaluate NO_2 VCD for comparison with GEMS data. Measurement was carried out from December 9, 2020, and it was either snowing or raining for more than half of the measurement period. For the validation of GEMS, Pandora data were averaged within ±10 minutes from the center of the GEMS observation time. The GEMS measurement pixels are not fixed but rather change as a function of time. Therefore, comparisons were made using~~performed at each Pandora location with the GEMS pixels~~ the ~~closet~~ GEMS pixels closet to each Pandora station. C~~The c~~omparisons wea~~a~~re carried between the NO_2 VCDs obtained from Pandora and GEMS ~~depending on the~~at CFs of 0.3, 0.5, and 0.7~~, respectively~~. The d~~D~~irect-sun DOAS (DS-DOAS) horizontal absorption path lengths are generally within 4 km~~,~~ with a solar zenith angle (SZA) < 50° (Herman et al., 2009). However, most ~~the~~ SZAs were ~~larger~~ greater than 50° during the campaign period. Thus, ~~the~~ a single GEMS pixel ~~sometimes~~ may not cover the absorption path of the Pandora observations. This horizontal discrepancy was partly considered ~~for~~ in the comparison between the Pandora NO_2 data and those of the GEMS, which can be found in ~~the~~ Section 4.3.

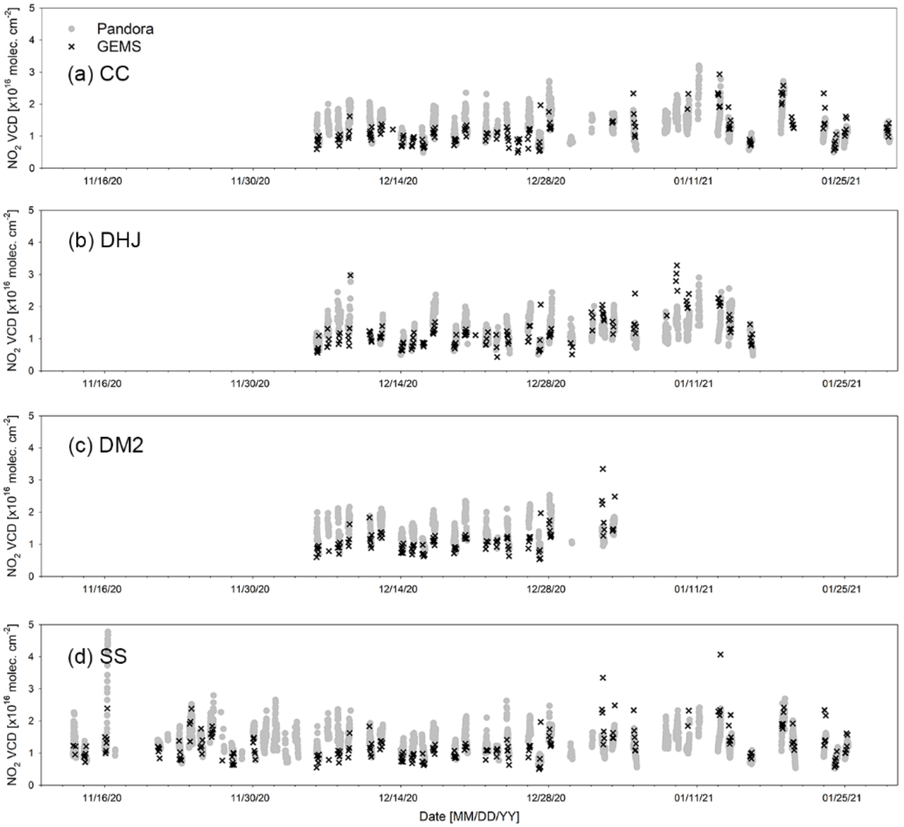
Pandora
GEMS
(a) CC
(b) DHJ
(c) DM2
(d) SS
NO2 VCD [x10^16 molec. cm^-2]
11/16/20
11/30/20
12/14/20
12/28/20
01/11/21
01/25/21
Date [MM/DD/YY]

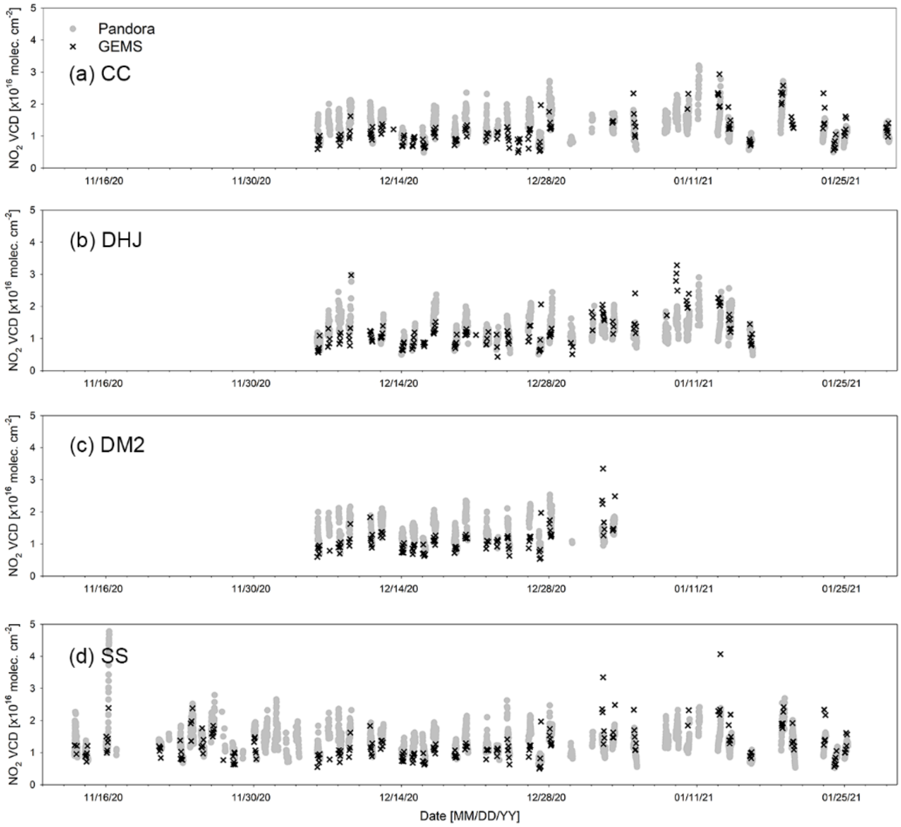

Figure 65. Hourly variations in NO_2 VCD obtained from Pandora (grey full circles) and GEMS (black **x**). (a), (b), (c), and (d) represent the CC, DHJ, DM2, and SS sites, respectively.

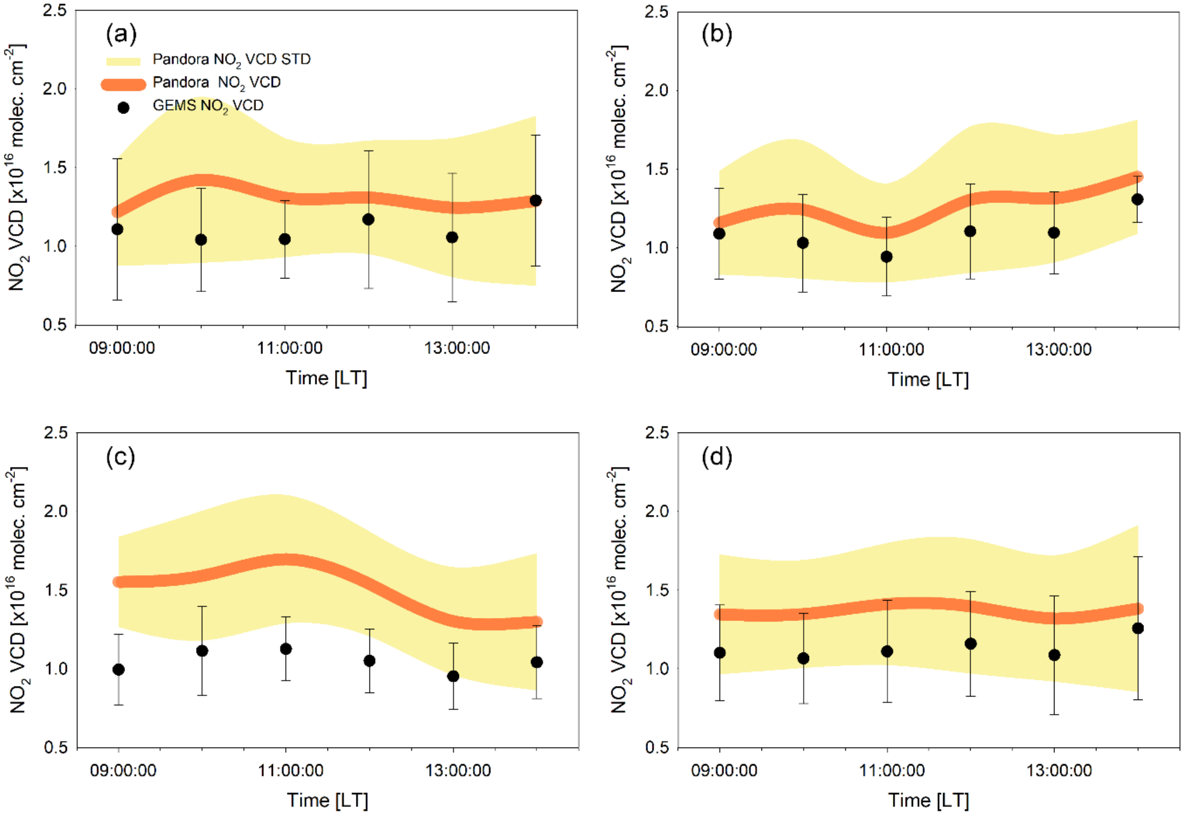
(a)
(b)
(c)
(d)
Pandora NO2 VCD STD
Pandora NO2 VCD
GEMS NO2 VCD
NO2 VCD [x10^16 molec. cm^-2]
Time [LT]
09:00:00
11:00:00
13:00:00
0.5
1.0
1.5
2.0
2.5

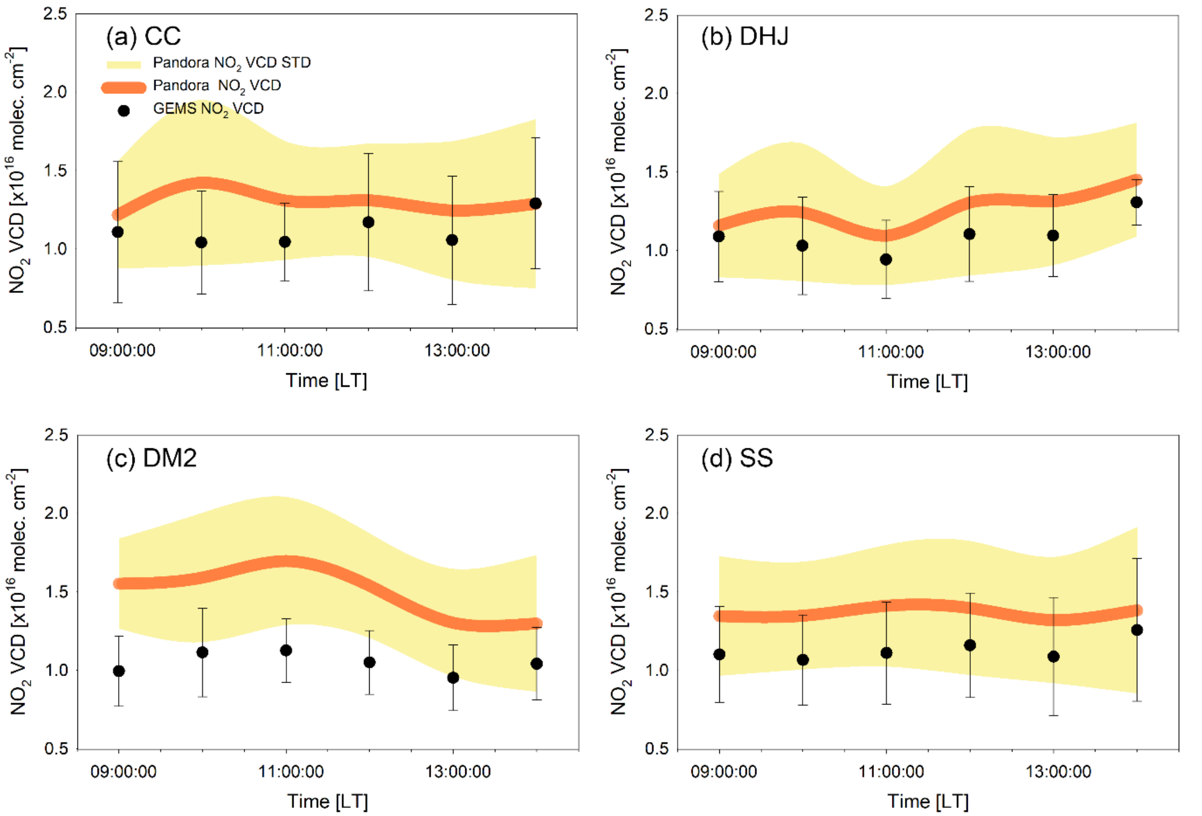

Figure 76. Hourly mean NO_2 VCD using only matched data from Pandora (orange line) and GEMS (black solid circles). (a), (b), (c), and (d) represent the CC, DHJ, DM2, and SS sites, respectively. Yellow shading represents the standard deviations of Pandora NO_2 VCD, and bars show those of GEMS; STD = standard deviation.

DailyThe hourly variations NO_2 VCD obtained from Pandora and GEMS are shown illustrated in Fig. 65 and compared for each of the four Seosan sites in Fig.ure 76. Figure 6 shows a good agreement between Pandora and GEMS fir all time periods. Since the GEMS measures six times in winter (10:00 – 15:00), but the Pandora NO_2 VCDs were retrieved from sunrise to sunset when SZA was less than 80°, Pandora NO_2 VCDs has slightly more widespread trend. In Fig. 7, the Ddifferences in the diurnal Pandora NO_2 VCD variations among the sites imply the inhomogeneity of the spatial tropospheric NO_2 columns over the sites. The hourly characteristics observed at the DHJ site could possibly be affected possibly by emissions from the petrochemical complex located approximatelybout 16 km northwest of in a north westerly direction from the site (see Fig. 1). It seems that tThere appears to beis a discrepancy in the NO_2 peaks observed from Pandora and GEMS at the CC site, where GEMS shows the enhanced NO_2 columns at 12:00 and 14:00 LT. The NO_2 columns observed from GEMS are found to show their hourly patterns similar to those from Pandora at the DHJ site. At the DM2 site, we found a good agreement between the NO_2 columns observed from Pandora and GEMS. At the DM2 site, the Pandora and GEMS VCD patterns were consistent, with both displaying peaks at 11:00 LT, followed by a decreasing trend. Overall, the NO_2 VCD from Pandora and GEMS showed ~~negligible~~ hourly variations, although those ~~o~~from Pandora tended to have slightly higher values than those ~~o~~from GEMS. There could be several reasons for this difference, ~~as~~ which are discussed later. Further quantitative comparisons of~~n~~ the Pandora and GEMS data were performed~~carried out~~, as discussed below. ~~In order to understand the correlation between Pandora and GEMS, the quantitative comparison was further performed.~~

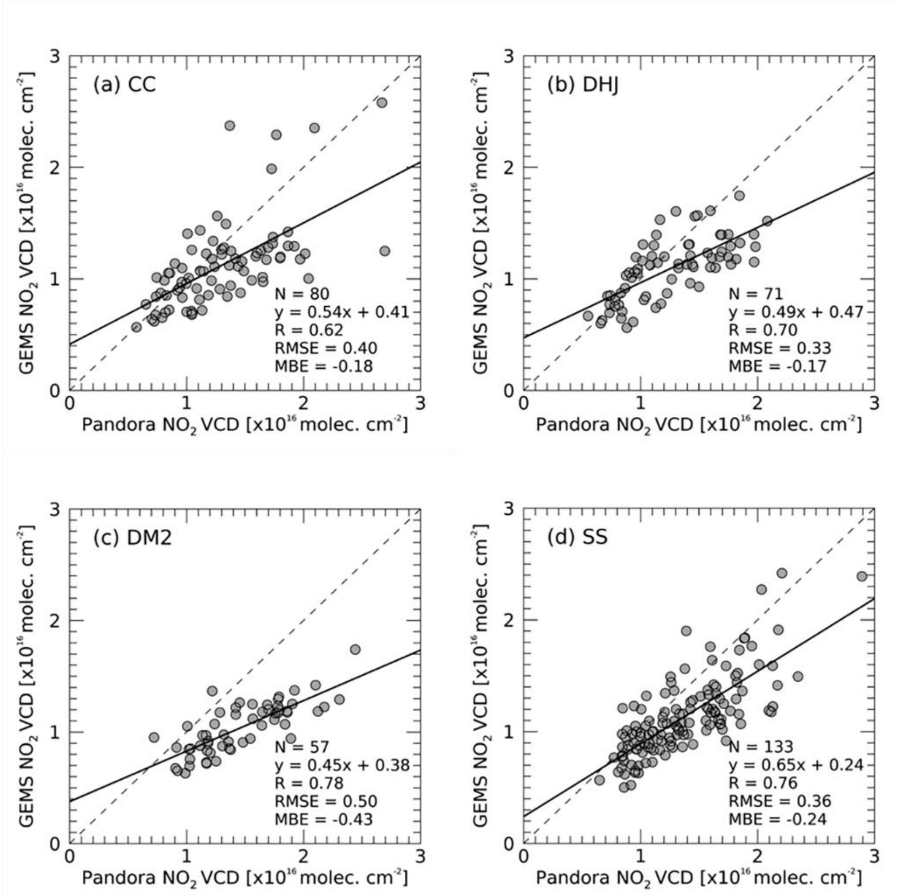
(a) CC
N = 80
y = 0.54x + 0.41
R = 0.62
RMSE = 0.40
MBE = -0.18
(b) DHJ
N = 71
y = 0.49x + 0.47
R = 0.70
RMSE = 0.33
MBE = -0.17
(c) DM2
N = 57
y = 0.45x + 0.38
R = 0.78
RMSE = 0.50
MBE = -0.43
(d) SS
N = 133
y = 0.65x + 0.24
R = 0.76
RMSE = 0.36
MBE = -0.24
GEMS NO2 VCD [x10^16 molec. cm^-2]
Pandora NO2 VCD [x10^16 molec. cm^-2]

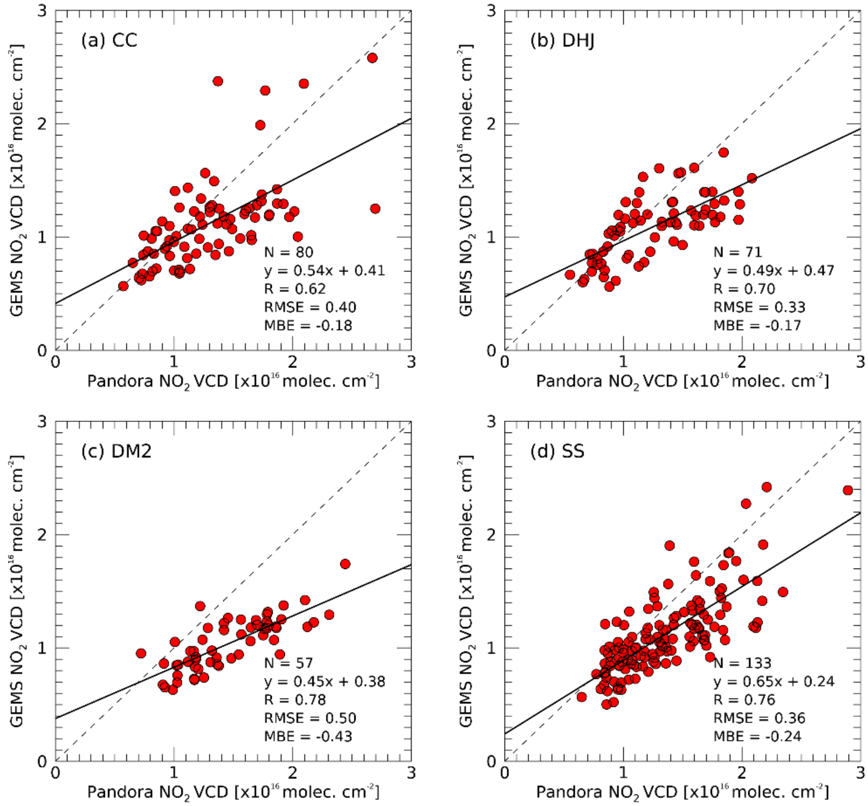

Figure 87. The scatterplot of NO_2 VCD between Pandora and GEMS in the CF < 0.3. (a), (b), (c) and (d) represent the CC, DHJ, DM2, and SS sites, respectively. The grey dashed line represents the 1:1 line and the black solid line represents the regression line.

Figure 87 shows the correlations between the NO_2 VCD for the Pandora and GEMS measurements at the four Seosan sites are shown in with Fig. 8 for CF of < 0.3. The R values are range from 0.620 and 0.78, with values of 0.62, 0.70, 0.78, and 0.76 at the CC, DHJ, DM2, and SS sites and slopes of 0.54, 0.49, 0.45, and 0.65, respectively. Although these comparisons were conducted over a short time period, the NO_2 VCD retrieved from the geostationary GEMS measurements showeds good correlations with those observed from ground-based Pandora measurement sites. The root mean square errors (RMSE) of the GEMS NO_2 against Pandora were 0.40, 0.33, 0.50, and 0.36 at the CC, DHJ, DM2, and SS sites, respectively, while the mean bias errors weare -0.18, -0.17, -0.43 and -0.24, respectively.

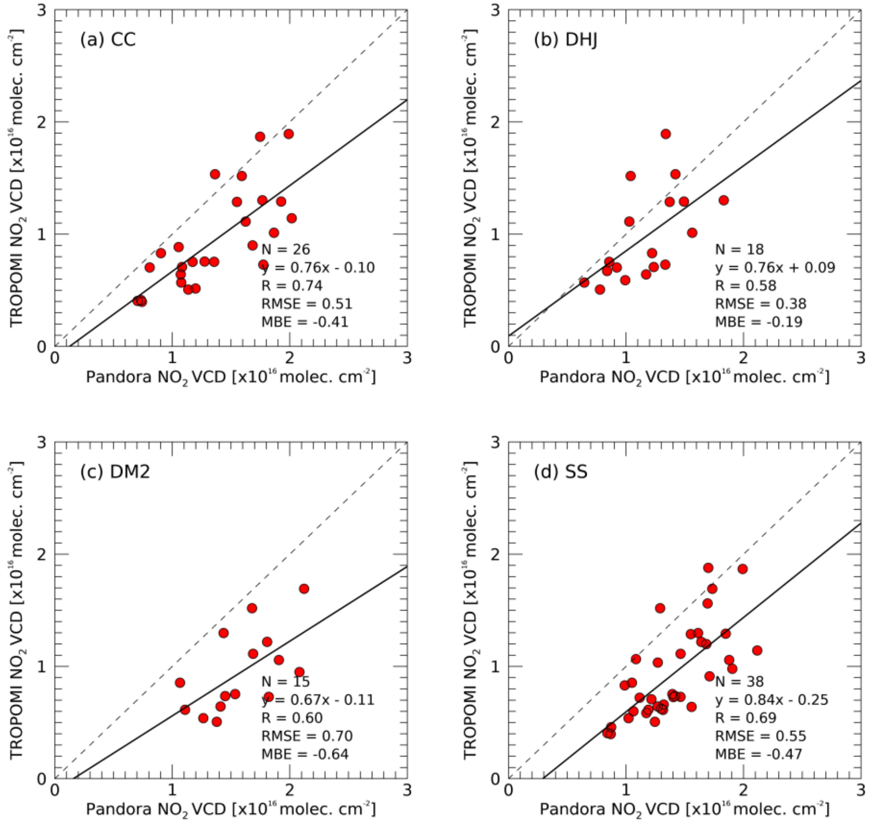

Figure 9. The scatterplot of NO_2 VCD between Pandora and TROPOMI. (a), (b), (c) and (d) represent the CC, DHJ, DM2, and SS site, respectively. The grey dashed line represents the 1:1 line and the black solid line represents the regression line.

In this study, an additional comparison was conducted with the LEO satellite TROPOMI.the TROPOMI NO_2 total columns ofused for comparison with Pandora NO_2 are the offline channel (OFFL) dataset with a quality assurance (QA) value larger than 0.75 and a Ccloud radiance fraction less than 0.3 used and compared with Pandora NO_2. The correlation coefficients between NO_2 total column from Pandora and TROPOMI are shown in Fig. 9 and are range from 0.58 to 0.74. For the CC, DHJ, DM2 and SS sites, RMSE of the TROPOMI NO_2 against Pandora are calculated to be 0.51, 0.38, 0.70, and 0.52 and MBE weare -0.42, -0.19, -0.64, and -0.46, respectively. In the case of GEMS, the RMSE was slightly smaller than that of TROPOMI, and there was a tendency toward underestimatione less.

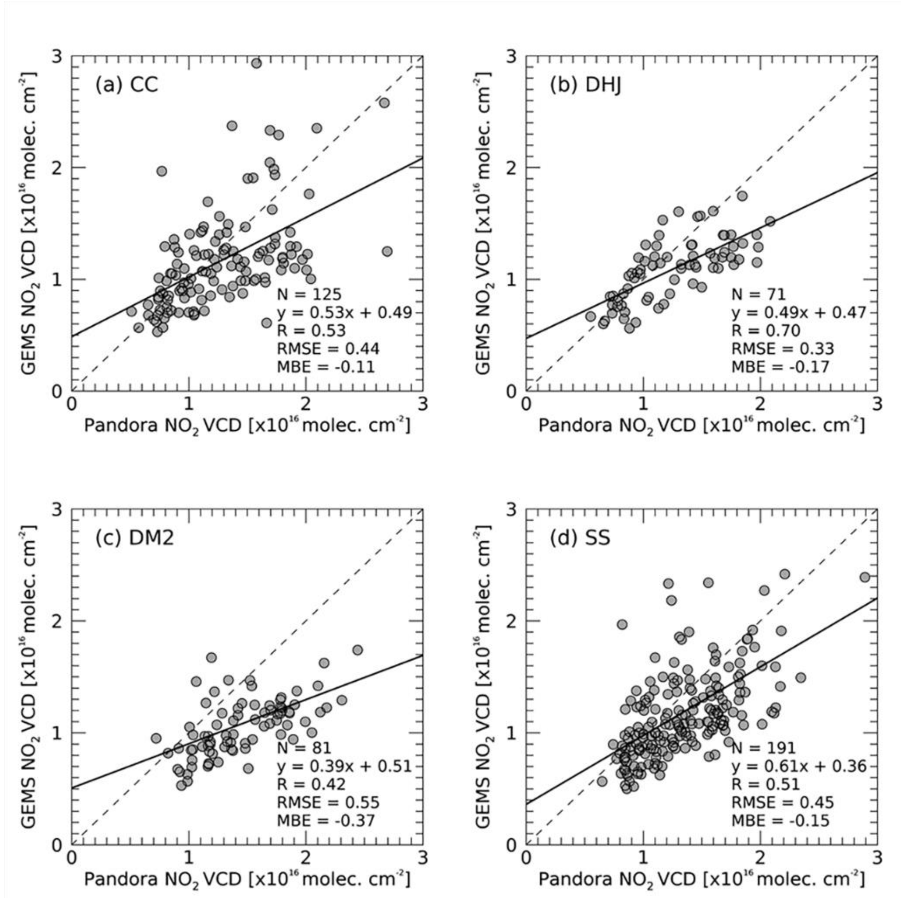
(a) CC
N = 125
y = 0.53x + 0.49
R = 0.53
RMSE = 0.44
MBE = -0.11
(b) DHJ
N = 71
y = 0.49x + 0.47
R = 0.70
RMSE = 0.33
MBE = -0.17
(c) DM2
N = 81
y = 0.39x + 0.51
R = 0.42
RMSE = 0.55
MBE = -0.37
(d) SS
N = 191
y = 0.61x + 0.36
R = 0.51
RMSE = 0.45
MBE = -0.15
GEMS NO2 VCD [x10^16 molec. cm^-2]
Pandora NO2 VCD [x10^16 molec. cm^-2]

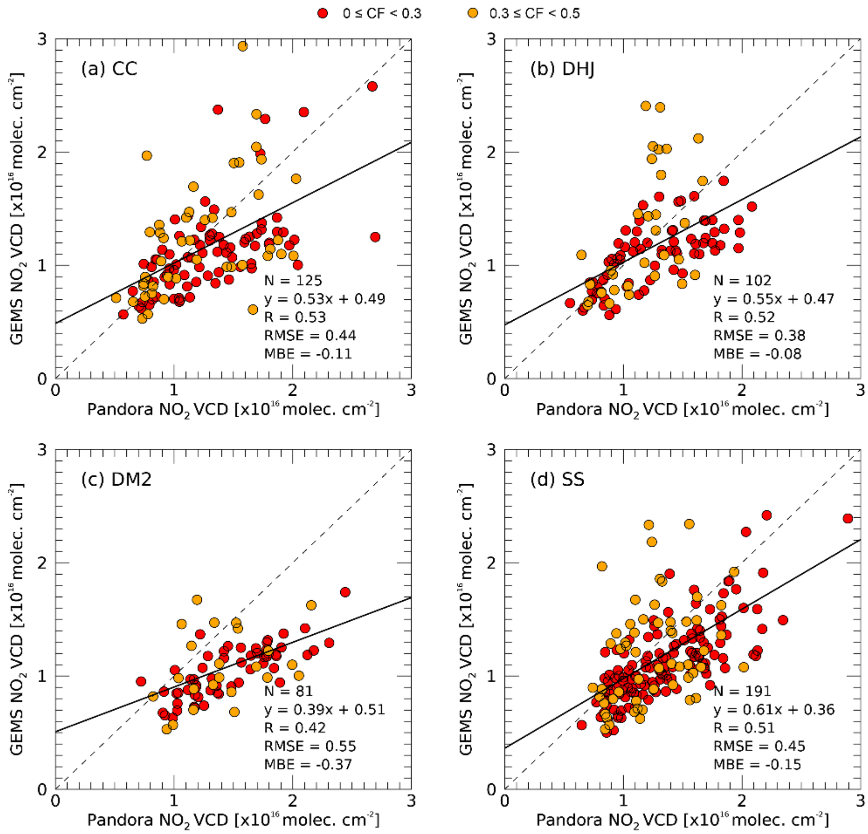

Figure 108. The scatterplot of NO_2 VCD between Pandora and GEMS in the CF conditions < 0.5 (a), (b), (c) and (d) represent the CC, DHJ, DM2, and SS sites, respectively. The grey dashed line represents the 1:1 line and the black solid line represents the regression line.

Figure 108 and 119 shows the correlations between the NO_2 VCD obtained from the Pandora and GEMS measurements with the CF < 0.5 and < 0.7, respectively. R values tends to decrease with the increasing CF value and are in the ranges of 0.42–0.53 for CF < 0.5 and 0.35–0.48 for CF < 0.7, with slopes of 0.53, 0.55, 0.39, and 0.612 and 0.54, 0.62, 0.38, and 0.62 at the CC, DHJ, DM2, and SS sites, respectively. The RMSE of the GEMS NO_2 VCD against the Pandora NO_2 values tendeds to increase with high CF value and the correlation coefficient decreaseds (Fig. 130). The hHigh correlation coefficient and low RMSE in the low CF conditions indicate that the diurnal NO_2 variations observed by the GEMS weare consistent with those of Pandora underin less cloudy conditions. The tendency of the correlation coefficient and RMSE against the variations inof the CF conditions implies that the enhanced cloud conditions may degrade the sensitivity of the GEMS measurement to NO_2 molecules present below or at the cloud layers. However, given the discrepancies among the NO_2 VCD from the four Pandora instruments at the same SS location, especially in under cloudy conditions (CF>0.3; Fig. 45), the weaker correlations between the GEMS and Pandora data underat higher CF conditions may be partly due to the uncertainties in the Pandora NO_2 VCD at high CF.

Variations inof MBE with CF are illustrated can be seen in Fig. 130, showing that the negative bias of GEMS against Pandora generally decreaseds with increasing CF. Indeed, a positive bias was observed at the DHJ site with the CF < 0.7. Except for the DM2 site, the magnitudes of the negative bias atin the high CF value (< 0.7) weare quite small in comparedison with those at CF < 0.3. The iIncreasing negative bias in GEMS NO_2 compared against that of in Pandora could be associated with the GEMS CF, which wasare used to calculate the GEMS NO_2 AMF. Regarding the Pandora NO_2 VCD as being closer to the true values than those of the GEMS, the large negative bias of the GEMS at low CF implies that the GEMS might underestimate the GEMS CF value, as measurement pixels with true CFs should be small. An underestimated GEMS CF may lead to an increase in the AMF and eventually to anthe underestimation of the NO_2 VCD in the pixels. Further investigation is required to identify the relationship between the GEMS CF and the negative bias tendency of the GEMS NO_2 VCD underin less cloudy conditions.

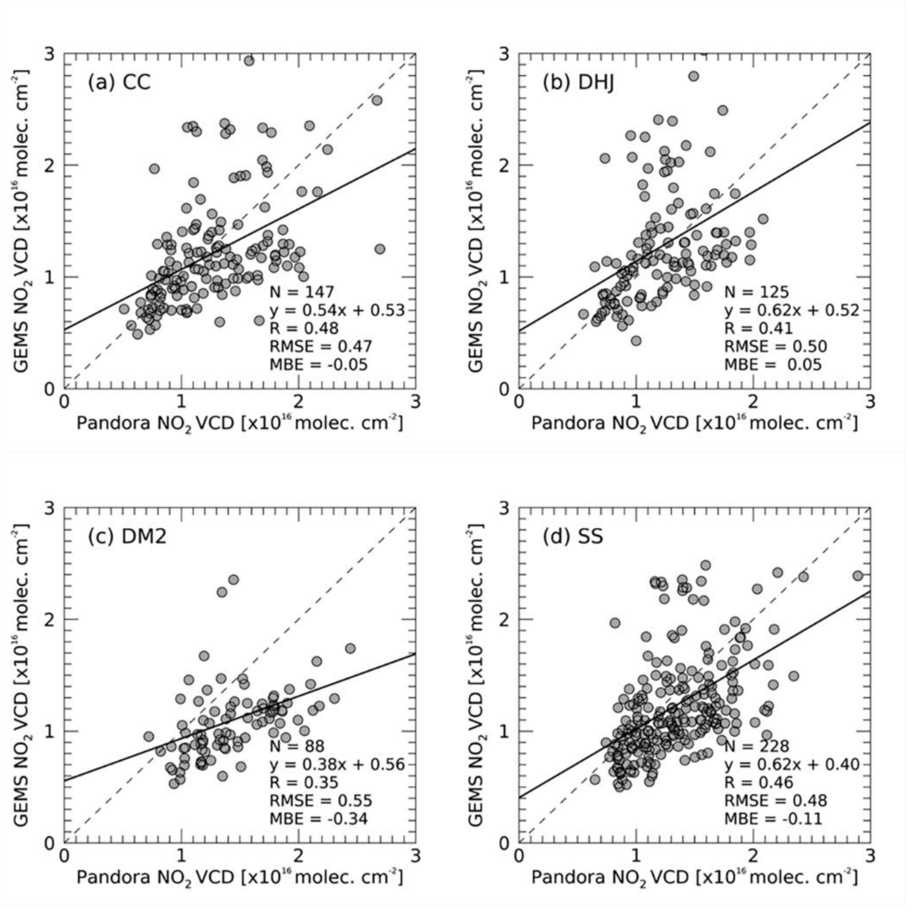
(a) CC
N = 147
y = 0.54x + 0.53
R = 0.48
RMSE = 0.47
MBE = -0.05
(b) DHJ
N = 125
y = 0.62x + 0.52
R = 0.41
RMSE = 0.50
MBE = 0.05
(c) DM2
N = 88
y = 0.38x + 0.56
R = 0.35
RMSE = 0.55
MBE = -0.34
(d) SS
N = 228
y = 0.62x + 0.40
R = 0.46
RMSE = 0.48
MBE = -0.11
GEMS NO2 VCD [x10^16 molec. cm^-2]
Pandora NO2 VCD [x10^16 molec. cm^-2]

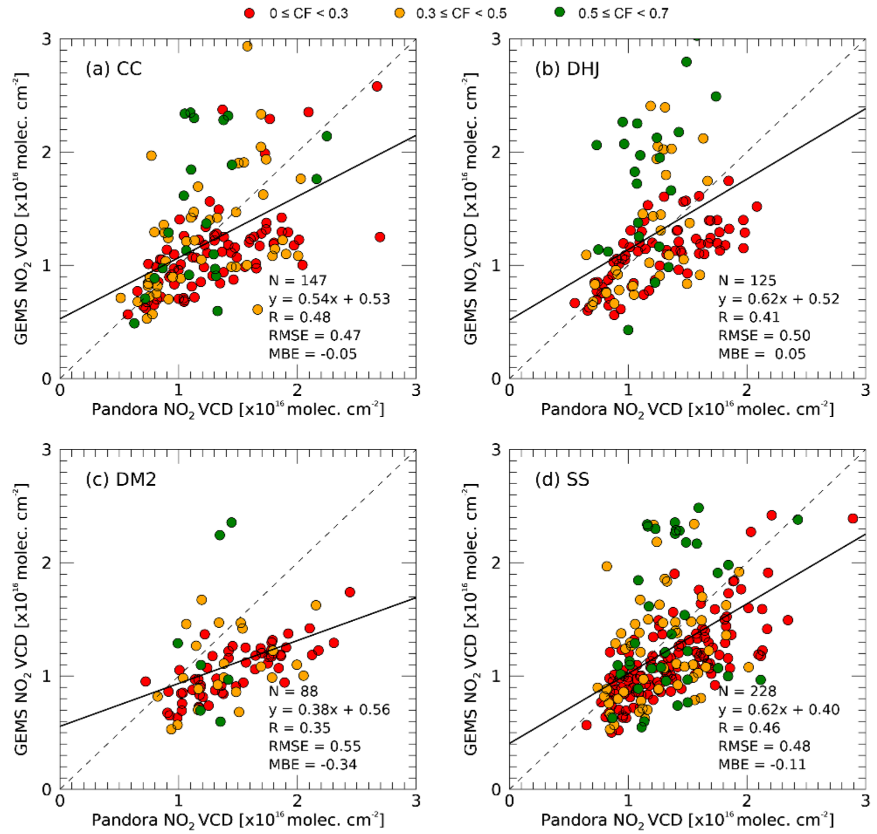

Figure 11~~9~~. The scatterplot of NO_2 VCD between Pandora and GEMS in the CF conditions < 0.7. (a), (b), (c) and (d) represent the CC, DHJ, DM2, and SS sites, respectively. The grey dashed line represents the 1:1 line and the black solid line represents the regression line.

4.3 Correction of horizontal representativeness

The GEMS pixel closest to the Pandora instrument location was used to assess the correlation between the Pandora and GEMS NO_2 VCD, as shown in Figs 9~~7~~–11~~9~~. The GEMS does not always observe the same measurement geometry, and the location of each GEMS pixel varies depending on the measurement schedule. The GEMS pixels close to the~~a~~ location where Pandora wa~~i~~s installed did~~oes~~ not ~~match~~ completely match the Pandora observation coverage.~~,~~ ~~so t~~Therefore, ~~is a~~ differences occur~~s~~ between ~~their~~ spatial coverage~~s~~. In particular, the NO_2 dSCD of Pandora wa~~i~~s obtained from an absorption light path between the ~~S~~sun and the instrument at the surface. ~~It is likely that the photons on a light path between Sun and Pandora are absorbed and scattered by both the NO_2 molecules at the lower troposphere in a pixel of the Pandora location and those at rather higher troposphere and stratosphere in the adjoining GEMS pixels, which are located on an azimuth angle connecting Sun and Pandora. Thus, we have attempted to account for the horizontal representativeness of the Pandora observation.~~The photons from the sun reaching Pandora may pass through more than one GEMS pixel, depending on the observation geometries of the measurements.

Figure 12 shows the variation in the measurement geometry of the Pandora instrument with the position of the sun. As the sun moves from east to west (morning to afternoon; (a) to (c) in Fig. 12), the direction of viewing path of the Pandora instrument changes. The GEMS pixels corresponding to the observation path of the Pandora instrument also differ. Horizontal effects were considered using GEMS pixels and distance ratios that changed according to the observation direction, as follows: First, we selected two pixels of the GEMS,; one closest pixel to the Pandora site and another pixel closest to the line of sight (i.e., closest to the viewing azimuth angle of the Pandora measurements). Here, we assumed that most of the NO_2 wais vertically distributed below 2 km altitude based on the airborne in-situ NO_2 measurements. The weighted mean values of the GEMS NO_2 accounting for the horizontal representativeness, are were calculated as follows:

$$\mathrm{VCD_{hr}} = \frac{d_2 \mathrm{VCD_1} + d_1 \mathrm{VCD_2}}{d_1 + d_2},$$

where $\mathrm{VCD_{hr}}$ is the NO_2 VCD accounting for the horizontal representativeness, the d_1 and d_2 are the distances between the Pandora and the center of the two GEMS pixels (1 denotes the closest pixel and 2 denotes the pixel to the line of sight), and VCD_1 and VCD_2 are the GEMS NO_2 VCD of the two pixels.

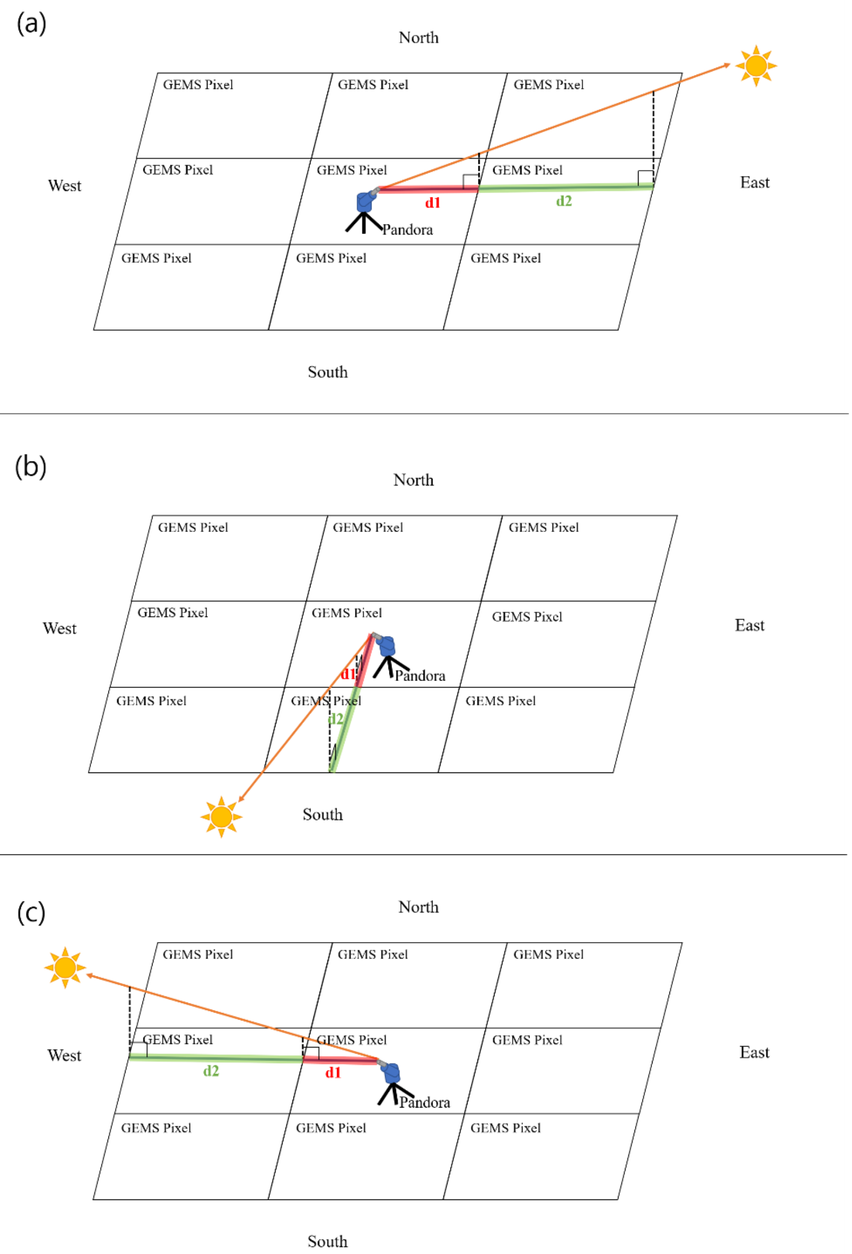

Figure 12. light path changes according to Pandora direct sun measurement geometry. (a), (b) and (c) represents morning, noon, and afternoon hours, respectively.

Figure 14~~1~~ shows the correlations between the NO_2 VCD from Pandora and the GEMS data which were corrected for the horizontal representativeness of Pandora at CF < 0.3. The correlation coefficients we~~a~~re found 0.69–0.81, which we~~a~~re higher than those without the correction of the horizontal representativeness; the R values at the CC, DHJ, DM2, and SS sites were 0.70, 0.69, 0.81, and 0.75, respectively. Correlations at two sites CC and DM2, ~~are~~ increased with ~~the~~ horizontal representativeness relative to those without ~~the~~ correction, whereas correlations at the DHJ and SS sites were similar with or without ~~the~~ correction. RMSEs were 0.37, 0.32, 0.49, and 0.36 with the correction, generally lower than 0.40, 0.33, 0.50, and 0.36 without the correction at the CC, DHJ, DM2, and SS sites, respectively. MBEs with the correction were similar to those without, with values of -0.18, -0.16, -0.43, and -0.2, at the CC, DHJ, DM2, and SS sites, respectively.

The viewing direction of the Pandora instrument changes depending on the location of sun (see Fig. 12). In the case of CC, Pandora observed the downtown area from morning to noon and the rural area on afternoon. The DM2 site observes in rural areas in the morning and downtown areas from noon. In this case, the correlation can be improved by correcting the horizontal effect, compared to using only the nearby GEMS pixel. In contrast, the reason for the lack of significant changes in agreement before and after considering the horizontal effect in the DHJ and SS appear to be that the regional characteristics are the same according to the viewing direction. The variability of the Pandora NO_2 VCD with the location at a single GEMS pixel has not yet been investigated in Seosan. However, as shown by the diurnal NO_2 characteristics at the four sites, the NO_2 VCD is~~are~~ likely to vary depending on the instrument location at a single GEMS pixel, causing ~~the~~ inherent discrepancies between the GEMS and Pandora~~.~~, which ~~The correction of horizontal representativeness~~ may ~~thus~~ partly account for the discrepancies between the horizontal and vertical measurement coverages of Pandora and GEMS. The range of statistical change was not large, but the correlation between GEMS and Pandora changed when the horizontal correction was applied to four places. Therefore, further investigations under long-term conditions and with a large number of sites are required.~~Overall, better GEMS–Pandora correlation and lower RMSEs were achieved using the correction for horizontal representativeness.~~

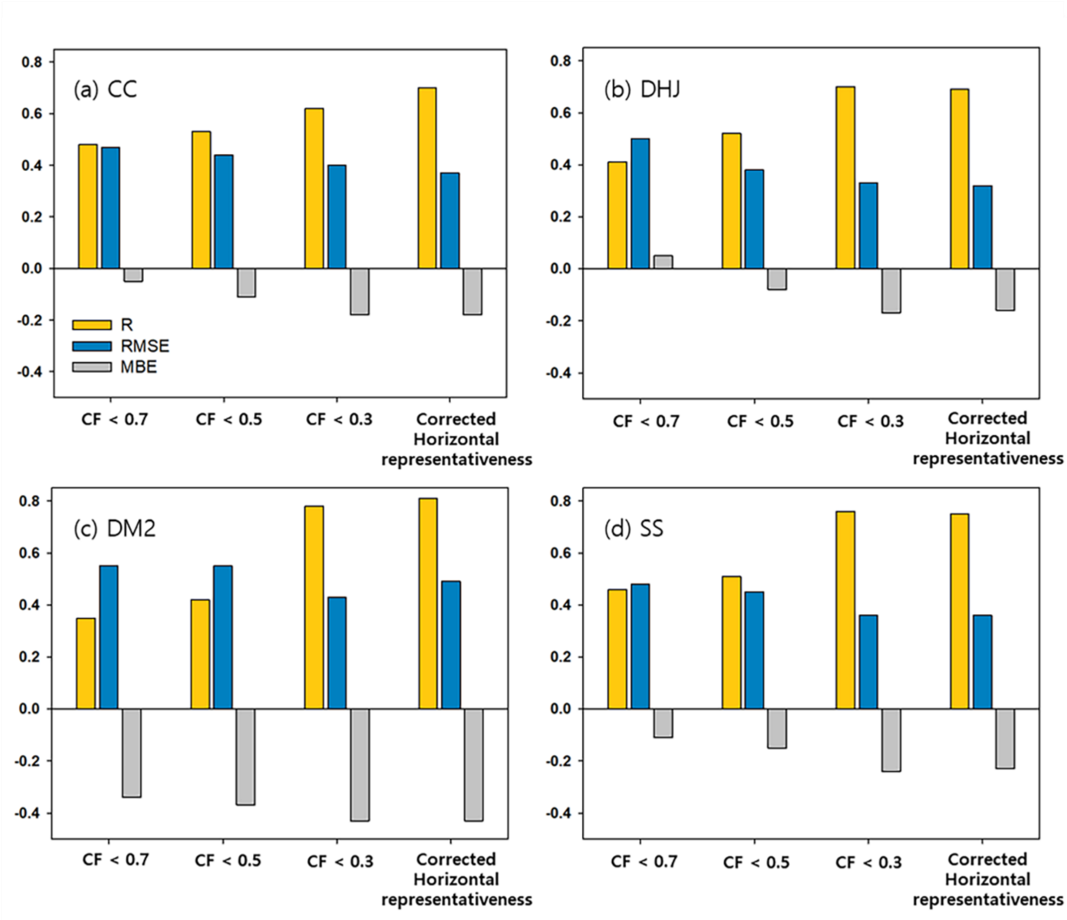
(a) CC
(b) DHJ
(c) DM2
(d) SS
R
RMSE
MBE
0.8
0.6
0.4
0.2
0.0
-0.2
-0.4
CF < 0.7
CF < 0.5
CF < 0.3
Corrected Horizontal representativeness

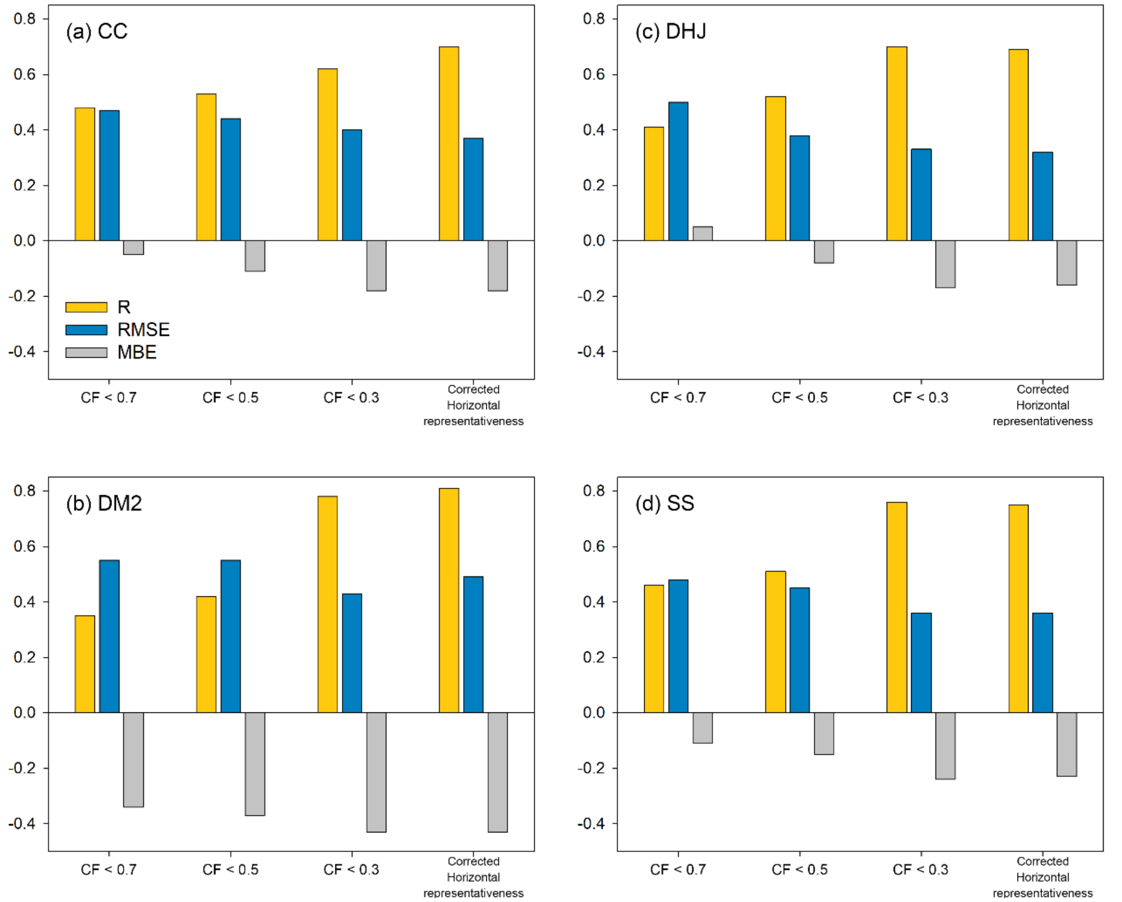

Figure 13~~0~~. R, RMSE, and MBE between NO_2 VCDs obtained from Pandora and GEMS depending on the CF conditions at (a), (b), (c) and (d), which represent~~s~~ the CC, DHJ, DM2, and SS sites, respectively.

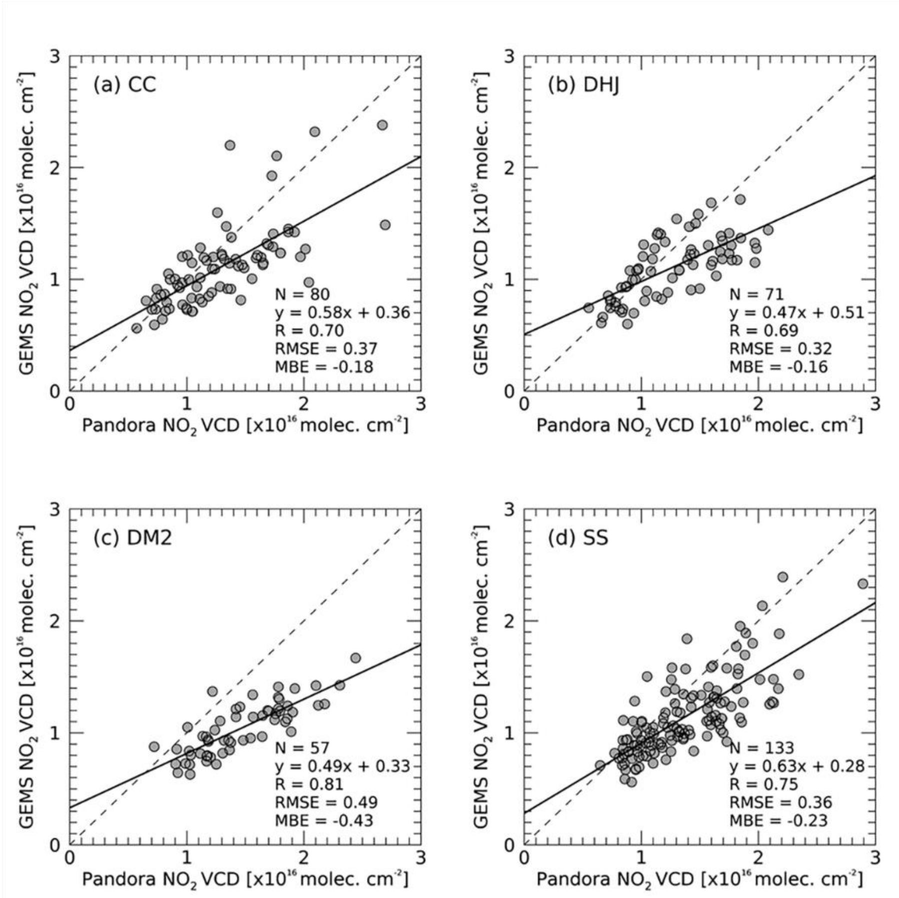

(a) CC
N = 80
y = 0.58x + 0.36
R = 0.70
RMSE = 0.37
MBE = -0.18
(b) DHJ
N = 71
y = 0.47x + 0.51
R = 0.69
RMSE = 0.32
MBE = -0.16
(c) DM2
N = 57
y = 0.49x + 0.33
R = 0.81
RMSE = 0.49
MBE = -0.43
(d) SS
N = 133
y = 0.63x + 0.28
R = 0.75
RMSE = 0.36
MBE = -0.23
GEMS NO2 VCD [x10^16 molec. cm^-2]
Pandora NO2 VCD [x10^16 molec. cm^-2]

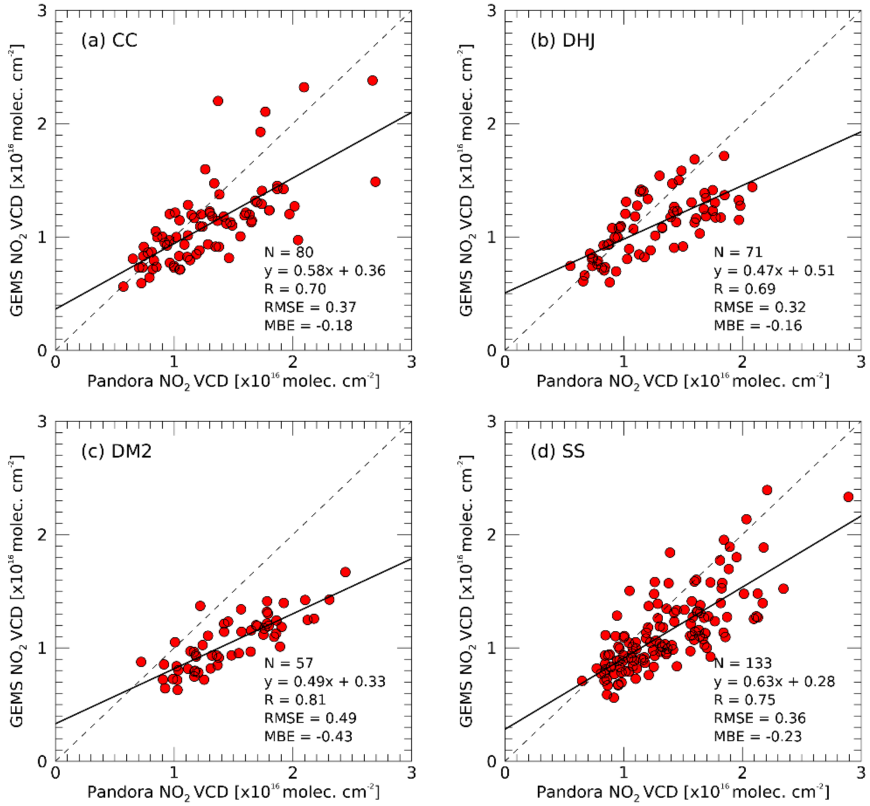

Figure 14~~1~~. The scatterplot of NO_2 VCD between Pandora and GEMS with the correction for the horizontal representativeness. (a), (b), (c) and (d) represent the CC, DHJ, DM2, and SS sites, respectively. The grey dashed line represents the 1:1 line and the black solid line represents the regression line.

5. Conclusion

The~~A~~ first evaluation of GEMS NO_2 was conducted~~carried out via~~ by comparison with ~~the~~ NO_2 data obtained from ~~the~~ ground-based Pandora measurements at four sites in Seosan, Korea. An intercomparison of NO_2 VCD among the four Pandora instruments revealed a slightly decreasing agreement among instruments with increasing CF, which could partly contribute ~~partly~~ to an inherent discrepancy between the GEMS and Pandora systems at high CF. It was observed that the correlations of ~~the~~ GEMS ~~NO2~~ NO_2 showed~~s a~~ good agreement ~~against~~ with those of Pandora ~~in~~ under~~a~~ less cloudy conditions (CF < 0.3). Higher correlation coefficients and lower RMSE were observed at lower CF conditions, indicating ~~the~~ a higher sensitivity of GEMS to hourly variations in atmospheric NO_2 concentrations under less-cloudy conditions. The NO_2 VCDs may differ between GEMS and Pandora for several reasons. First, NO_2 cross sections at 220 K and 254.4 K were used for NO_2 retrieval from GEMS and Pandora, respectively. PGN methods of NO_2 retrieval can lead to overestimation or underestimation depending on where tropospheric or stratospheric NO_2 is predominantly present (Verheolst et al., 2021). Second, there is a difference in the spatial resolution of GEMS and Pandora. However, the overall correlations or patterns between the GEMS and Pandora were very similar. We also ~~have~~ attempted to account for the horizontal representativeness of ~~the~~ Pandora observations. The m~~M~~ean correlations at the four sites increased with correction for horizontal representativeness, with maximum correlation (R = 0.81) and minimum correlation (R = 0.69) at the DM2 and DHJ sites, respectively. Variations in~~of~~ the correlations between sites may be attributed to variability ~~of~~ in the NO_2 VCD observed by Pandora, depending on the instrument located at a single GEMS pixel. This suggests that the influence of NO_2 source on the observation direction can be considered by correcting for the horizontal effect. The NO2 VCDs from GEMS, Pandora, and TROPOMI were compared for the first time. However, GEMS data (version 1.0) were used and the comparison period was short. Recently, data from GEMS, version 2.0 were provided by the NIER. Long-term validation using GENS version 2.0 data should be conducted in future studies.

Author contributions. DK and SK retrieved and analyzed NO_2 VCDs from Pandora and designed the study, while participating in the campaign. HH, LC, HL, Deok-rae K, Donghee K, JY, DL, UJ, WC and KL planned, organized and performed the Seosan campaign. UJ, CS, SK, SP, JK, and TFH provided and supported instrument management. JK and JP provided GEMS NO_2 data and supported the validation process. All authors reviewed and discussed this paper.

Competing interests. The authors declare that they have no conflict of interest.

References

Bechle, M. J., Millet, D. B., and Marshall, J. D.: Remote sensing of exposure to NO2, satellite versus ground-based measurement in a large urban, Atmos. Environ., 69, 345–353, https://doi.org/10.1016/j.atmosenv.2012.11.046, 2013.

Boersma, K. F., Jacob, D. J., Trainic, M., Rudich, Y., DeSmedt, I., Dirksen, R., and Eskes, H. J.: Validation of urban NO2 concentrations and their diurnal and seasonal variations observed from the SCIAMACHY and OMI sensors using in situ surface measurements in Israeli cities, Atmos. Chem. Phys., 9, 3867–3879, https://doi.org/10.5194/acp-9-3867-2009, 2009

Bovensmann, H., Burrows, J. P., Buchwitz, M., Frerick, J., Noël, S., Rozanov, V. V., Chance, K. V., and Goede, A. P. H.: SCIAMACHY: Mission objectives and measurement modes, J. Atmos. Sci., 56, 127–150, https://doi.org/10.1175/1520-0469(1999)056<0127:SMOAMM>2.0.CO;2, 1999.

Burrows, J., Weber, M., Buchwitz, M., Rozanov, V., LadstatterWeißenmayer, A., Richter, A., Debeek, R., Hoogen, R., Bramstedt, K., Eichmann, K.-U., and Eisinger, M.: The Global Ozone Monitoring Experiment (GOME): Mission concept and first scientific results, J. Atmos. Sci., 56, 151–175, https://doi.org/10.1175/1520-0469(1999)056<0151:TGOMEG>2.0.CO;2, 1999.

Cede, A., Mueller, M., Tiefengraber, M., Abuhassan, N., and Williams, D.: Evaluating the impact of spatial resolution on tropospheric NO2 column comparisons within urban areas using highresolution airborne data, Atmos. Meas. Tech., 12, 6091–6111, https://doi.org/10.5194/amt-12-6091-2019, 2019.

Choi, Y., Kim, G., Kim, B., Kwon, M.: Geostationary Environment Monitoring Spectrometer (GEMS) Algorithm Theoretical Basis Document Cloud Retrieval Algorithm, available at: https://nesc.nier.go.kr/ko/html/satellite/doc/doc.do, (last access: 5 June 2023), 2020.

Crutzen, Paul J.: The role of NO and NO2 in the chemistry of the troposphere and stratosphere, Annu. Rev. Earth Planet. Sci., 7, 443-472, https://doi.org/10.1146/annurev.ea.07.050179.002303, 1979.

Fayt, C., De Smedt, I., Letocart, V., Merlaud, A., Pinardi, G., and Van Roozendael, M.: QDOAS Software user manual, available at: https://uv-vis.aeronomie.be/software/QDOAS/QDOAS_manual.pdf (last access: 24 March 2022), 2011.

Herman, J. R., Cede, A., Spine, E., Mount, G., Tzortziou, M., and Abuhassan, N.: NO2 column amounts from ground-based Pandora and MFDOAS spectrometers using the direct-sun DOAS technique: Intercomparisons and application to OMI validation, J. Geophys. Res., 114, D13307, https://doi.org/10.1029/2009JD011848, 2009.

Herman, J., Spinei, E., Fried, A., Kim, J., Kim, J., Kim, W., Cede, A., Abuhassan, N., and Segal-Rozenhaimer, M.: NO2 and HCHO measurements in Korea from 2012 to 2016 from Pandora spectrometer instruments compared with OMI retrievals and with aircraft measurements during the KORUS-AQ campaign, Atmos. Meas. Tech., 11, 4583–4603, https://doi.org/10.5194/amt-11-4583-2018, 2018.

Herman, J., Abuhassan, N., Kim, J., Kim, J., Dubey, M., Raponi, M., and Tzortziou, M.: Underestimation of column NO2 amounts from the OMI satellite compared to diurnally varying ground-based retrievals from multiple PANDORA spectrometer instruments, Atmos. Meas. Tech., 12, 5593–5612, https://doi.org/10.5194/amt-12-5593-2019, 2019.

Hong, H., Lee, H., Kim, J., Jeong, U., Ryu, J., Lee, D. S.: Investigation of Simultaneous Effects of Aerosol Properties and Aerosol Peak Height on the Air Mass Factors for Space-Borne NO2 Retrievals, Remote Sens., 9, 208, https://doi.org/10.3390/rs9030208, 2017.

Honninger, G., von Friedeburg, C., and Platt, U.: Multi axis differential optical absorption spectroscopy (MAX-DOAS), Atmos.Chem. Phys., 4, 231–254, 2004.

Irie, H., Kanaya, Y., Akimoto, H., Iwabuchi, H., Shimizu, A., and Aoki, K.: First retrieval of tropospheric aerosol profiles using MAX-DOAS and comparison with lidar and sky radiometer measurements, Atmos. Chem. Phys., 8, 341–350, https://doi.org/10.5194/acp-8-341-2008, 2008.

Jeong, U., Tsay, S.-C., Giles, D. M., Holben, B. N., Swap, R. J., Abuhassan, N., and Herman, J. R.: The SMART-s Trace Gas and Aerosol Inversions: I. Algorithm Theoretical Basis for Column Property Retrievals, J. Geophys. Res.-Atmos., 125, e2019JD32088, https://doi.org/10.1029/2019JD032088, 2020.

Jeong, U., Hong, H.: Assessment of Tropospheric Concentrations of NO2 from the TROPOMI/Sentinel-5 Precursor for the Estimation of Long-Term Exposure to Surface NO2 over South Korea, Remote Sens. 13 1877, https://doi.org/10.3390/rs13101877, 2021.

Judd, L. M., Al-Saadi, J. A., Janz, S. J., Kowalewski, M. G., Pierce, R. B., Szykman, J. J., Valin, L. C., Swap, R., Cede, A., Mueller, M., Tiefengraber, M., Abuhassan, N., and Williams, D.: Evaluating the impact of spatial resolution on tropospheric NO2 column comparisons within urban areas using highresolution airborne data, Atmos. Meas. Tech., 12, 6091–6111, https://doi.org/10.5194/amt-12-6091-2019, 2019.

Judd, L. M., Al-Saadi, J. A., Szykman, J. J., Valin, L. C., Janz, S. J., Kowalewski, M. G., Eskes, H. J., Veefkind, J. P., Cede, A., Mueller, M., Gebetsberger, M., Swap, R., Pierce, R. B., Nowlan, C. R., Abad, G. G., Nehrir, A., and Williams, D.: Evaluating Sentinel-5P TROPOMI tropospheric NO2 column densities with airborne and Pandora spectrometers near New York City and Long Island Sound, Atmos. Meas. Tech., 13, 6113–6140, https://doi.org/10.5194/amt-13-6113-2020, 2020.

Kim, J., Jeong, U., Ahn, M.-H., Kim, J. H., Park, R. J., Lee, H., Song, C. H., Choi, Y.-S., Lee, K.-H., Yoo, J.-M., Jeong, M.-J., Park, S. K., Lee, K.-M., Song, C.-K., Kim, S.-W., Kim, Y. J., Kim, S.-W., Kim, M., Go, S., Liu, X., Chance, K., Miller, C. C., Al-Saadi, J., Veihelmann, B., Bhartia, P. K., Torres, O., Abad, G. G., Haffner, D. P., Ko, D. H., Lee, S. H., Woo, J.-H., Chong, H., Park, S. S., Nicks, D., Choi, W. J., Moon, K.-J., Cho, A., Yoon, J., Kim, S.-K., Hong, H., Lee, K., Lee, H., Lee, S., Choi, M., Veefkind, P., Levelt, P. F., Edwards, D. P., Kang, M., Eo, M., Bak, J., Baek, K., Kwon, H.-A., Yang, J., Park, J., Han, K. M., Kim, B.-R., Shin, H.-W., Choi, H., Lee, E., Chong, J., Cha, Y., Koo, J.-H., Irie, H., Hayashida, S., Kasai, Y., Kanaya, Y., Liu, C., Lin, J., Crawford, J. H., Carmichael, G. R., Newchurch, M. J., Lefer, B. L., Herman, J. R., Swap, R. J., Lau, A. K. H., Kurosu, T. P., Jaross, G., Ahlers, B., Dobber, M., McElroy, C. T., and Choi, Y.: New era of air quality monitoring from space, Geostationary Environment Monitoring Spectrometer (GEMS), B. Am. Meteorol. Soc., 101, E1–E22, https://doi.org/10.1175/BAMS-D-18-0013.1, 2020.

Lamsal, L. N., Krotkov, N. A., Celarier, E. A., Swartz, W. H., Pickering, K. E., Bucsela, E. J., Gleason, J. F., Martin, R. V., Philip, S., Irie, H., Cede, A., Herman, J., Weinheimer, A., Szykman, J. J., and Knepp, T. N.: Evaluation of OMI operational standard NO2 column retrievals using in situ and surface-based NO2 observations, Atmos. Chem. Phys., 14, 11587–11609, https://doi.org/10.5194/acp-14-11587-2014, 2014.

Levelt, P. F., Hilsenrath, E., Leppelmeier, G. W., van den Oord, G. B. J., Bhartia, P. K., Tamminen, J., de Haan, J. F., and Veefkind, J. P.: Science Objectives of the Ozone Monitoring Instrument, IEEE T. Geosci. Remote, 44, 1199–1208, https://doi.org/10.1109/TGRS.2006.872333, 2006.

Li, J., Wang, Y., Zhang, R., Smeltzer, C., Weinheimer, A., Herman, J., Boersma, K. F., Celarier, E. A., Long, R. W., Szykman, J. J., Delgado, R., Thompson, A. M., Knepp, T. N., Lamsal, L. N., Janz, S. J., Kowalewski, M. G., Liu, X., and Nowlan, C. R.: Comprehensive evaluations of diurnal NO2 measurements during DISCOVER-AQ 2011: effects of resolution-dependent representation of NOx emissions, Atmos. Chem. Phys., 21, 11133–11160, https://doi.org/10.5194/acp-21-11133-2021, 2021.

Munro, R., Lang, R., Klaes, D., Poli, G., Retscher, C., Lindstrot, R., Huckle, R., Lacan, A., Grzegorski, M., Holdak, A., Kokhanovsky, A., Livschitz, J., and Eisinger, M.: The GOME2 instrument on the Metop series of satellites: instrument design, calibration, and level 1 data processing – an overview, Atmos. Meas. Tech., 9, 1279–1301, https://doi.org/10.5194/amt-9-1279-2016, 2016.

Park, J., Lee, H., Hong, H.: Geostationary Environment Monitoring Spectrometer (GEMS) Algorithm Theoretical Basis Document NO2 Retrieval Algorithm, available at: https://nesc.nier.go.kr/product/document?page=1&limit=10, (last access: 24 March 2022), 2020.

Pinardi, G., Van Roozendael, M., Hendrick, F., Theys, N., Abuhassan, N., Bais, A., Boersma, F., Cede, A., Chong, J., Donner, S., Drosoglou, T., Dzhola, A., Eskes, H., Frieß, U., Granville, J., Herman, J. R., Holla, R., Hovila, J., Irie, H., Kanaya, Y., Karagkiozidis, D., Kouremeti, N., Lambert, J.-C., Ma, J., Peters, E., Piters, A., Postylyakov, O., Richter, A., Remmers, J., Takashima, H., Tiefengraber, M., Valks, P., Vlemmix, T., Wagner, T., and Wittrock, F.: Validation of tropospheric NO2 column measurements of GOME-2A and OMI using MAX-DOAS and direct sun network observations, Atmos. Meas. Tech., 13, 6141–6174, https://doi.org/10.5194/amt-13-6141-2020, 2020.

Seinfeld, J. H. and Pandis, S. N.: Atmospheric Chemistry and Physics: From Air Pollution to Climate Change, John Wiley & Sons, Inc., 1998.

Serdyuchenko, A., Gorshelev, V., Weber, M., Chehade, W., and Burrows, J. P.: High spectral resolution ozone absorption cross-sections – Part 2: Temperature dependence, Atmos. Meas. Tech.,7, 625–636, https://doi.org/10.5194/amt-7-625-2014, 2014.

Thalman, R. and Volkamer, R.: Temperature dependant absorption cross-sections of O2−O2 collision pairs between 340 and 630 nm at atmospherically relevant pressure Phys. Chem. Chem. Phys., 15, 15371–15381, doi: 10.1039/C3CP50968K, 2013.

Tzortziou, M., Herman, J. R., Ahmad, Z., Loughner, C. P., Abuhassan, N., and Cede, A.: Atmospheric NO2 dynamics and impact on ocean color retrievals in urban nearshore regions, J. Geophys. Res.-Oceans, 119, 3834–3854, https://doi.org/10.1002/2014JC009803, 2014.

Tzortziou, M., Herman, J. R., Cede, A., Loughner, C. P., Abuhassan, N., and Naik, S.: Spatial and temporal variability of ozone and nitrogen dioxide over a major urban estuarine ecosystem, J. Atmos. Chem., 72, 287–309, https://doi.org/10.1007/s10874-013-9255-8, 2015.

Vandaele, A., Hermans, C., Simon, P., Carleer, M., Colin, R., Fally, S., M'erienne, M., Jenouvrier, A., and Coquart, B.: Measurements of the NO2 absorption cross-section from 42 000 cm−1 to 10 000 cm−1 (238–1000 nm) at 220 K and 294 K, J. Quant. Spectrosc. Ra., 59, 171–184, https://doi.org/10.1016/s0022-4073(97)00168-4, 1998.

Veefkind, J. P., Aben, I., McMullan, K., Förster, H., de Vries, M., Otter, G., Claas, J., Eskes, H. J., de Haan, J. F., Kleipool, Q.L., van Weele, M., Hasekamp, O., Hoogeveen, R., Landgraf, J., Snel, R., Tol, P., Ingmann, P., Voors, R., Kruizinga, B., Vink, R., Visser, H., Levelt, P. F., and de Vries, J.: TROPOMI on the ESA Sentinel-5 Precursor: A GMES mission for global observations of the atmospheric composition for climate, air quality and ozone layer applications, Remote Sens. Environ., 120, 70–83 https://doi.org/10.5194/amt-13-6113-2020, 2012.

Verhoelst, T., Compernolle, S., Pinardi, G., Lambert, J.-C., Eskes, H. J., Eichmann, K.-U., Fjæraa, A. M., Granville, J., Niemeijer, S., Cede, A., Tiefengraber, M., Hendrick, F., Pazmiño, A., Bais, A., Bazureau, A., Boersma, K. F., Bognar, K., Dehn, A., Donner, S., Elokhov, A., Gebetsberger, M., Goutail, F., Grutter de la Mora, M., Gruzdev, A., Gratsea, M., Hansen, G. H., Irie, H., Jepsen, N., Kanaya, Y., Karagkiozidis, D., Kivi, R., Kreher, K., Levelt, P. F., Liu, C., Müller, M., Navarro Comas, M., Piters, A. J. M., Pommereau, J.-P., Portafaix, T., Prados-Roman, C., Puentedura, O., Querel, R., Remmers, J., Richter, A., Rimmer, J., Rivera Cárdenas, C., Saavedra de Miguel, L., Sinyakov, V. P., Stremme, W., Strong, K., Van Roozendael, M., Veefkind, J. P., Wagner, T., Wittrock, F., Yela González, M., and Zehner, C.: Ground-based validation of the Copernicus Sentinel-5P TROPOMI NO2 measurements with the NDACC ZSL-DOAS, MAX-DOAS and Pandonia global networks, Atmos. Meas. Tech., 14, 481–510, https://doi.org/10.5194/amt-14-481-2021, 2021.

Wagner, T., Beirle, S., Brauers, T., Deutschmann, T., Frieß, U., Hak, C., Halla, J. D., Heue, K. P., Junkermann, W., Li, X., Platt, U., and Pundt-Gruber, I.: Inversion of tropospheric profiles of aerosol extinction and HCHO and NO2 mixing ratios from MAX-DOAS observations in Milano during the summer of 2003 and comparison with independent data sets, Atmos. Meas. Tech., 4, 2685–2715, https://doi.org/10.5194/amt-4-2685-2011, 2011.

Wang, Y., Beirle, S., Lampel, J., Koukouli, M., De Smedt, I., Theys, N., Li, A., Wu, D., Xie, P., Liu, C., Van Roozendael, M., Stavrakou, T., Müller, J.-F., and Wagner, T.: Validation of OMI, GOME-2A and GOME-2B tropospheric NO2, SO2 and HCHO products using MAX-DOAS observations from 2011 to 2014 in Wuxi, China: investigation of the effects of priori profiles and aerosols on the satellite products, Atmos. Chem. Phys., 17, 5007–5033, https://doi.org/10.5194/acp-17-5007-2017, 2017.

Zhao, X., Griffin, D., Fioletov, V., McLinden, C., Cede, A., Tiefengraber, M., Müller, M., Bognar, K., Strong, K., Boersma, F., Eskes, H., Davies, J., Ogyu, A., and Lee, S. C.: Assessment of the quality of TROPOMI high-spatial-resolution NO2 data products in the Greater Toronto Area, Atmos. Meas. Tech., 13, 2131–2159, https://doi.org/10.5194/amt-13-2131-2020, 2020.